Perspectives for Next Generation Lithium-ion Battery Cathode Materials

Samuel G. Booth,[1,14,a,b)] Alisyn J. Nedoma,[1,14,a,b)] Nirmalesh N. Anthonisamy,[1,14] Peter J. Baker,[2,14] Rebecca Boston,[3,14] Hugo Bronstein,[4,14] Simon J. Clarke,[5,14] Edmund J. Cussen,[1,3,14] Venkat Daramalla,[6,14] Michael De Volder,[7,14] Siân E. Dutton,[6,14] Viktoria Falkowski,[5,14] Norman Fleck,[8,14] Harry S. Geddes,[5,14] Naresh Gollapally,[1,14] Andrew L. Goodwin,[5,14] John M. Griffin,[9,14] Abby R. Haworth,[9,14] Michael A Hayward,[5,14] Stephen Hull,[2,14] Beverley J. Inkson,[3,14] Beth J. Johnston,[1,14] Ziheng Lu,[10,14] Judith L. MacManus-Driscoll,[10,14] Xabier Martínez De Irujo Labalde,[5,14] Innes McClelland,[1,2,14] Kirstie McCombie,[3,14] Beth Murdock,[9] Debasis Nayak,[10,14] Seungkyu Park,[7,14] Gabriel E. Pérez,[2,14] Chris J. Pickard,[10,14] Helen Y. Playford,[2,14] Simon Price,[11] David O. Scanlon,[12,13,14] Joe C. Stallard,[8,14] Nuria Tapia-Ruiz,[9,14] Anthony R. West,[3,14] Laura Wheatcroft,[3,14] Megan Wilson,[11] Li Zhang,[9,14] Xuan Zhi,[3] Bonan Zhu,[12,14] and Serena A. Corr[1,3,14,b)]

[1] Department of Chemical and Biological Engineering, University of Sheffield, Sheffield, S1 3JD, UK
[2] ISIS Neutron & Muon Source, STFC Rutherford Appleton Laboratory, Didcot, OX11 0QX, UK
[3] Department of Materials Science and Engineering, The University of Sheffield, Sheffield, S1 3JD, UK
[4] Department of Chemistry, University of Cambridge, Cambridge, CB2 1EW, UK
[5] Department of Chemistry, University of Oxford, Inorganic Chemistry Laboratory, Oxford, OX1 3QR, UK
[6] Cavendish Laboratory, University of Cambridge, Cambridge, CB3 0HE, UK
[7] Institute for Manufacturing, Department of Engineering, University of Cambridge, Cambridge, CB3 0FS, UK
[8] Department of Engineering, University of Cambridge, Cambridge, CB2 1PZ, UK
[9] Department of Chemistry, Lancaster University, Lancaster, LA1 4YB, UK
[10] Department of Materials Science and Metallurgy, University of Cambridge, Cambridge, CB3 0FS, UK
[11] Exawatt, Sheffield, S10 2LR, UK
[12] Department of Chemistry, University College London, London, WC1H 0AJ, UK
[13] Diamond Light Source Ltd., Diamond House, Harwell Science and Innovation Campus, Didcot, OX11 0DE, UK
[14] The Faraday Institution, Quad One, Harwell Campus, OX11 0RA, UK
(a) These authors contributed equally to this work
(b) Corresponding authors: s.g.booth@sheffield.ac.uk, a.nedoma@sheffield.ac.uk and s.corr@sheffield.ac.uk

Abstract

Transitioning to electrified transport requires improvements in sustainability, energy density, power density, lifetime and cost of lithium-ion batteries, with significant opportunities remaining in the development of next-generation cathodes. This presents a highly complex, multiparameter optimisation challenge, where developments in cathode chemical design and discovery, theoretical and experimental understanding, structural and morphological control, synthetic approaches and cost reduction strategies can deliver performance enhancements required in the near- and longer-term. This multifaceted challenge requires an interdisciplinary approach to solve, which has seen the establishment of numerous academic and industrial consortia around the world to focus on cathode development. One such example is the Next Generation Lithium-ion Cathode

Materials project, FutureCat, established by the UK's Faraday Institution for electrochemical energy storage research in 2019, aimed at developing our understanding of existing and newly-discovered cathode chemistries. Here, we present our perspective on persistent fundamental challenges, including protective coatings and additives to extend lifetime and improve interfacial ion transport, the design of existing, and the discovery of new cathode materials where cation and cation-plus-anion redox-activity can be exploited to increase energy density, the application of earth-abundant elements which could ultimately reduce costs and the delivery of new electrode topologies resistant to fracture which can extent battery lifetime.

Contents

1. Why the Cathode Matters
2. Current State of the Art: High Nickel Content Layered Cathodes
3. High Voltage through Spinel Materials
4. High Capacity through Disordered Rocksalts
5. Sustainable Alternative Chemistries
6. Searching for New Materials through Crystal Structure Prediction
7. Enhancing Lifetime through Gradient and Core Shell Structures
8. Enhancing Performance through Hierarchical Structuring
9. Understanding the Role of Interfaces
10. Advances in Operando Characterisation of Cathodes
    (i) Structural Analysis
    (ii) Understanding Disorder
    (iii) Establishing Diffusion Properties
    (iv) Understanding the Interplay between Morphology and Performance
11. Cathode Mechanical Strength Properties and Testing
12. Acknowledgements
13. References

Introduction

Samuel G. Booth, Alisyn J. Nedoma and Serena A. Corr

Electric-vehicle (EV) batteries presage a step change from internal combustion engines (ICE) to electric motors, offering lower running costs and reduced carbon emissions. Next-generation lithium-ion batteries will be largely driven by technological innovations in the cathode that will enable higher energy densities and also present opportunities for cost reduction since cathode materials remain the bottleneck to cost parity. Transformative cathode technology must meet a range of specifications including higher capacity and power, longer first-lifetime, safer construction, sustainable sourcing of materials, lower cost, and greener manufacturing processes. Lithium-ion systems provide the highest specific energy density of current battery technologies; however, the cathode contributes substantially to both the cost and mass of the assembled unit. Cathode materials exhibit lower capacity relative to current commercially applied anode materials and therefore represent a limiting factor for electrochemical performance. Cathode formulations also often comprise low-abundancy transition metals that are costly and may pose ethical concerns in the supply chain. A multi-objective approach to the development of cathode materials is therefore necessary to holistically streamline the design, synthesis, processing and scale-up of lithium-ion batteries.

Efforts to address these challenges have seen the establishment of vibrant research consortia around the world, including the Faraday Institution FutureCat project in the UK, to pioneer the discovery and development of new cathode materials. Recognizing these challenges, we have established a research consortium which benefits from a depth of multidisciplinary expertise from within and extending beyond the battery field. Strong links have been formed with industrial collaborators to help solve industry-facing challenges and forge the interdisciplinary links to help bring next-generation materials to market. As this field continues to mature and materials development becomes more and more involved, we believe that there will be many developments as opposed to a one-size-fits-all solution. Instead, key advances in individual areas of study must be used to drive forward progress in all areas through a shared knowledge and expertise.

In this roadmap, we set out what we see as the challenges related to the most mature next-generation cathode materials, high nickel content layered metal oxides, disordered rocksalts and spinels, along with design principles that we suggest are important to consider when establishing new cathode chemistries based on green, earth-abundant minerals. Materials discovery can now be driven by the application of computational structure searching to amplify the value of experimental work. Morphological control of the cathode structure can enhance the capacity and longevity of batteries, including the development of gradient compositions to counteract operationally-induced cation migration as well as the production of hierarchical assemblies to fine tune the shape and size of cathode particles for optimal performance. We acknowledge that the development of new materials is continuously driven by the development of more sensitive measurement techniques. We explore the new insights that can be gleaned, particularly through *operando* measurements, to uncover the structure and mechanism of the functioning electrode at a range of length scales. Finally, we examine the interplay between chemical and mechanical mechanisms which cause a loss of active material and diminish cell performance over the lifetime of a battery. We envision that this combined approach will enable a step change in cathode performance that supports the decarbonisation of our energy and transport systems.

1. Why the Cathode Matters

Megan Wilson and Simon Price

All technologies that support decarbonisation through electrification – whether for energy generation, power conversion or energy storage – have a “figure of merit”: a metric that encapsulates their history, status and prospects on the technology roadmap and provides a common focus for the research community and manufacturing industries.

Generally this figure of merit relates in some way to cost reduction. In lithium-ion batteries, the figure of merit that matters most is the cost per kilowatt-hour, the manufacturing cost per unit of energy stored. This is typically stated in $/kWh. Driving this number down, while simultaneously ensuring that gravimetric and volumetric energy density targets are maintained, will be the critical factor in bringing EV technology to price parity with ICE vehicles.

As lithium-ion battery production continues to scale with the rapid growth of EVs, the driver of \$/kWh cost reduction will move from reducing the numerator – the total manufacturing cost – to increasing the denominator, cell performance. This is because the absolute manufacturing cost of the cell, battery pack or system eventually becomes limited by the fundamental costs of the bulk materials that increasingly dominate the cost structure. But metrics such as energy density will continue to improve as new approaches are found to eke out additional performance from existing and novel materials. Such cell performance increases also pay dividends at the pack and system levels. Cells account for about 70% of the cost of today's battery systems and, in broad terms, a 10% increase in cell storage capacity (for no increase in absolute cost) leads to a corresponding reduction not only in cell cost per kWh, but also in pack and system cost per kWh.

Moving inside the cell, the key drivers of cost per kWh are the anode and cathode energy density and raw materials costs. **Figure 1a** shows a conventional wet-electrolyte cell, using a standard graphite anode and a cathode chemistry at the leading edge of the mainstream: $LiNi_{0.8}Mn_{0.1}Co_{0.1}O_2$ (NMC811). For this particular configuration, the cathode active material accounts for a little over one-third of the cell mass and volume and, depending on the purchase price, about one-half of the cell cost. The anode active material, by contrast, occupies more of the cell volume, but less mass and just a fraction of the cost: one-fifth of the cost of the cathode active material and about one-tenth of the total cell cost.

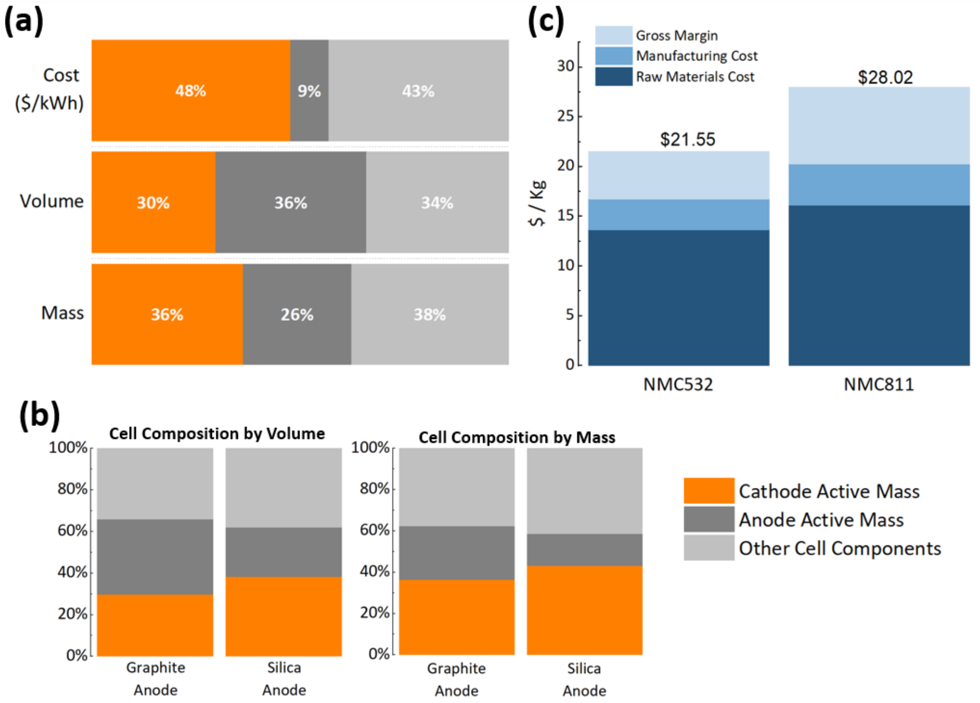

Figure 1. Composition of wet-electrolyte pouch cell. "Other" includes current collectors, separator, electrolyte, binders, cell casing and other minor components of the cell. b)

Impact of introducing a high energy density anode on the composition of the cell by volume and mass. c) Cathode active material price and cost structure for NMC532 and NMC811 based on manufacturer reports from China. Source Exawatt (2019 data).

Given the cathode's disproportionate influence on today's cell performance and cost, finding ways to "shrink" the cathode – in volume and mass, but particularly in cost – is perhaps the key challenge facing the battery industry. Cathode electrochemical performance has increased in recent years as the mainstream industry has shifted from lithium iron phosphate ($LiFePO_4$) and low-nickel to nickel-rich ternary materials such as NMC811. Much excitement in the industry today also focuses on the anode, particularly on "silicon-rich" anode technologies. The incorporation of silicon into conventional graphite anodes increases the energy capacity of the anode, shrinking the anode volume for a given cell capacity. While this improves the overall energy density of the cell, it also increases the relative amount of cathode active material in the cell (**Figure 1b**), exacerbating the challenge of reducing the cathode cost.

The raw material precursors of mainstream cathode active material variants already account for about 80% of the total cathode active material manufacturing cost at large-scale producers in China (**Figure 1c**). In other words, there is little room to reduce the cost of existing cathode raw materials by streamlining the materials manufacturing process. When considering novel cathode active materials, their absolute cost (in $/kg) can only be greater than that of conventional materials if they bring gains in performance that put them on parity, or better, than conventional materials in $/kWh terms.

Not only will the driver of future cost reduction ($/kWh) move from absolute manufacturing cost reductions to performance gains, it is critical that these performance gains are achieved without actually *increasing* the absolute manufacturing cost. This means that researchers, when developing novel cathode formulations, must carefully consider several factors relating to materials selection, including:

- Abundance and supply/demand. How much of each component material exists in the world and how accessible is it? How much of each material might be required by the battery industry today and in the long term? Which other industries compete for these materials and in what volumes, today and in the future?

- Extractability. How costly is the raw material to extract and refine? Can this be done sustainably and in an environmentally sound manner?

- Geopolitics and ethical considerations. Is the raw material a conflict mineral? Do certain countries or companies control the supply of it? Is the material already within the supply chain, or can it be sourced locally on an economically viable basis?

- Quality. How much battery-grade material is available and at what price? Are the impurity levels acceptable, or even excessive (i.e. could materials costs be reduced by using a lower-grade material of acceptable quality)?

- Processability. Can the materials be processed cheaply into the cathode active material and ultimately into the cell?

Choosing the optimal cathode materials need not require avoiding expensive components entirely. As long as these materials are used in small enough quantities, e.g. as dopants to bulkier, cheaper base materials, the overall cost per kWh can be reduced even if the absolute cost increases slightly.

By 2019, the manufacturing cost of goods sold utilizing lithium-ion cells had already fallen below $85/kWh for the leading producers in China, which equates to a reduction of approximately 20% in two years. With the cathode already accounting for more than one-third of the cell cost, and likely to account for closer to one-half with the emergence of high-performance anodes, the need for high-performance, affordable cathodes will only increase.

The cathode and anode are locked in a kind of technological arms race. Improvements to either electrode serve the ultimate goal of increasing cell energy density and reducing battery pack cost, but disproportionate progress in one electrode increases the demand on the other. While anodic developments remain vital and welcome to the industry, they will not solve the fundamental challenge facing cell manufacturers. Improving the cathode becomes ever more important as the key lever to increase cell energy density and reduce cell and system cost.

2. State of the Art: High Nickel Content Layered Cathodes

Beth J. Johnston, Naresh Gollapally and Serena A. Corr

Layered transition metal oxides, of general formula $LiMO_2$, continue to dominate the commercial lithium-ion battery market. Such compositions, with the α-$NaFeO_2$ structure, consist of distinct transition metal and lithium layers where the Li ions can be removed and inserted during charge and discharge respectively. The $LiCoO_2$ (LCO) structure,[1] utilised in the first commercialised lithium ion batteries in 1990, are still widely in use 30 years later in cell phones and other portable electronics; a testament to their groundbreaking success. However, several issues have been identified with LCO: thermal runaway at higher states of charge mandates strict safety limits[2] that cap the practical capacities of LCO to ~140 mAh g^{-1} and ethical and supply chain issues surround the mining practices of cobalt. These challenges have driven research in the direction of alternative and improved layered oxide compositions.

Substitution of the transition metal cations within these layered oxides has proven a pioneering strategy with the introduction of $LiNi_{1/3}Mn_{1/3}Co_{1/3}O_2$ (NMC111) where Ni^{2+}, Mn^{4+} and Co^{3+} are distributed across the transition metal layer (**Figure 2**).[3] Electrochemical activity arises from the redox behaviour of Ni^{2+} to Ni^{4+} while the Mn^{4+} remains electrochemically inactive but plays a vital role in structural stabilisation. There is debate surrounding the electrochemical activity of the Co^{3+} cations but Co also plays an important stabilising role.[4,5] Under typical cycling conditions, NMC111 can deliver specific capacities of approximately 160 mAh g^{-1}. However, it is estimated that an energy density of ≥ 800 Wh kg^{-1} at the cathode level (corresponding to ≥ 350 Wh kg^{-1} at the cell level for state-of-the-art cell constructions) is required to meet the higher energy densities demanded by electric vehicle applications.[6] Thus higher specific capacities at practical voltages are afforded by increasing the nickel content in these layered compositions with a particular interest in nickel-rich NMCs and NCAs *i.e.* $LiNi_xMn_yCo_{1-x-y}O_2$ and $LiNi_xCo_yAl_{1-x-y}O_2$ for $x \geq 0.8$, capable of delivering initial specific capacities ≥ 200 mAh g^{-1} at ~ 4.2 V *vs.* lithium. Alongside these nickel-rich compositions, there is also a renewed interest in pristine $LiNiO_2$ (LNO), which can deliver the largest specific capacity of these layered oxides at practical working potentials.[7] However, specific challenges arise for such nickel-rich compositions including synthetic complications and structural and thermal instabilities at high states of charge that drastically reduce their cycle life.

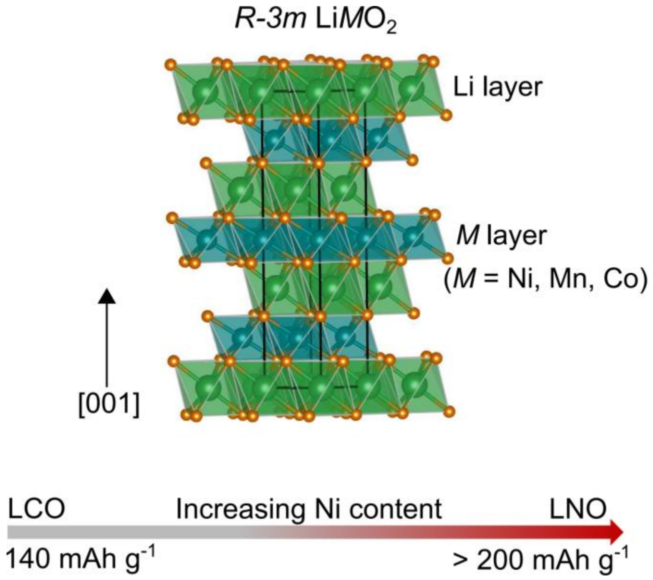

Figure 2. Crystal structure representation of R-3m $LiMO_2$ layered oxide (M = Ni, Co, Mn) showing the arrangement of Li and transition metal cations across separate layers. The specific capacities (at practical working potentials) improve upon increasing the Ni content.

The challenges facing the application of higher nickel content layered oxides span from an increasing complexity presented by synthetic conditions at higher nickel content, to structural and thermal instabilities initiated at higher states of charge (corresponding to larger degrees of delithiation). Upon moving to higher nickel compositions, reduced stability provides unique demands regarding synthesis and handling procedures particularly at scale. For example, the final calcination step requires an oxygen environment, expensive Li sources such as LiOH and stringent control of reaction times and temperatures depending on the desired composition. On an atomic level, synthetic challenges can also arise from cation mixing where the comparable ionic radii of Ni (0.69 Å) and Li (0.72 Å) can result in anti-site mixing across the layers. A similar off-stoichiometry is also observed during the synthesis of LNO, whereby structures of composition $Li_{1-z}Ni_{1+z}O_2$ are often obtained, with the excess Ni^{2+} ions occupying sites in the lithium layer. The presence of Ni^{2+} in the Li layer can block Li^+ ion diffusion pathways and cause local layer collapse during charge through cation shrinkage, which is manifested in a large irreversible capacity loss during the first cycle.[8]

The sensitive surface chemistry of these nickel-rich compositions presents additional requirements during handling and characterisation. Surface residual lithium species, which may affect charge-transfer resistance or promote gas generation on cycling (*e.g.* Li_2CO_3 and LiOH), may persist via reactions with CO_2, H_2O and O_2 and necessitate handling and storing under inert environments. These surface species may also influence chemical and structural observations drawn from surface sensitive analysis techniques.[9] Also associated with the increased surface reactivity are deleterious cathode–electrolyte reactions at high states of charge which may lead to an increasingly complex surface reaction layer containing LiF, inorganic and organic species.[10] Cycling to higher cut-off voltages also initiates surface reconstruction processes where the rhombohedral layered structure (*R-3m*) can irreversibly transform into spinel (*Fd-3m*) and/or rocksalt (*Fm-3m*) type surface phases. The decreased thermal stabilities arising from increased nickel content can also play a role through oxygen evolution from thermal lattice decomposition at highly delithiated states. As these processes generally take place at surfaces or interfaces, they are further intensified by the emergence of microcracks (and thus, fresh surfaces) that are generated by abrupt and anisotropic expansion and contraction of the lattice at voltages above 4.2 V.[11] These evolving surface changes may result in a loss of active cathode material and increased charge transfer resistance upon cycling which manifests in rapid capacity fade and drastically reduces the lifetime of these cathodes.

Mitigating the degradation processes that occur in nickel rich layered oxides is paramount in realising their full potential as high energy density cathodes. One strategy involves introducing electrochemically inactive dopant cations into the layered oxide structure. These dopants may be chosen to selectively substitute for either lithium or transition metal cations depending on the desired effect. For example, small amounts (*ca.* 1 to 5 mol%) of Mg^{2+} cations can be substituted into the lithium layer where they can provide a pillaring effect to enhance cycling stability. The Mg^{2+} ions successfully suppress the anisotropic lattice distortions occurring during cycling that lead to micro-crack generation.[12,13] Doping with Al^{3+} on the transition metal sites has also been widely reported in an effort to mitigate Ni migration and improve thermal stabilities.[14] Other dopants can also improve the surface chemistry of the cathodes whilst stabilising the bulk structure; for example, small amounts of W^{6+} doped into LNO have been observed to promote a rocksalt-type phase during synthesis which segregates to the particle surfaces where it acts to passivate side reactions. Thermal and structural stabilities also increased, leading to much improved cycling performance.[15,16] A similar effect was also observed for Zr-doped materials.[17] A rich variety of further dopants *e.g.* Na, Ca, Ti, Ta and Mo, including co-doping of Mg-Ti, have been shown to improve the cycling properties of high nickel content cathodes.[18-21] Looking forward, a seemingly vast selection of potential future dopants exist, warranting insights from computational methods to guide further synthetic targets, and technoeconomic analysis to ensure sustainability.

Implementing passivating surface layers to cathode particles to mitigate surface degradation processes is also commonly achieved through coating methods. An effective coating should be chemically and structurally stable during electrochemical cycling and should not impinge on the charge transport properties of the electrode. Popular coatings include metal oxides, for example MgO, Al_2O_3, SiO_2, TiO_2, ZnO, SnO_2 and ZrO_2.[22] There is also an interest in binary metal oxides that contain lithium as effective coatings for nickel rich materials e.g. Li_2SiO_3, $Li_4Ti_5O_{12}$, Li_2TiO_3, Li_2ZrO_3, Li_2MoO_4 and $Li_{0.5}La_{0.5}TiO_3$.[23] Wet coating methods using water or other solvents (e.g. ethanol) offer a cheap and scalable coating process whereas techniques such as atomic layer deposition (ALD) offer excellent control over the film thickness, uniformity and stoichiometry. ALD introduces cost and technological considerations so the process scalability must be considered.[24] Improved cycling stabilities of nickel rich NMCs and NCAs by coating with Al_2O_3 via an ALD process have been demonstrated.[25,26] Further detail on the influence of the CEI and interfaces is provided in subsequent sections. Additional strategies to enhance cycling properties in these materials include core-shell or gradient-like structures, and advanced particle engineering routes to suppress particle cracking by obtaining *e.g.* single crystal particles[27] or polycrystalline materials with specific grain crystallographic orientations.[28]

Development of single crystal layered transition metal oxides

Typically, polycrystalline arrangements of nickel-rich cathode materials are applied in current lithium-ion batteries consisting of agglomerated primary particles which form secondary assemblies. When formulating an electrode from such structures, the pressure applied during calendering can cause secondary particle cracking, increasing the electrode surface area exposed to the liquid electrolyte. The resulting growth in cathode-electrolyte-interface (CEI) may result in an increased charge transfer resistance. Additionally, during battery cycling, inter-granular fracture may disrupt Li-ion diffusion processes and result in the loss of active material leading to capacity fade.[29] The emergence of single crystal nickel-rich cathode particles are now opening up the possibility of greater resistance to crack formation during electrode processing and operation.

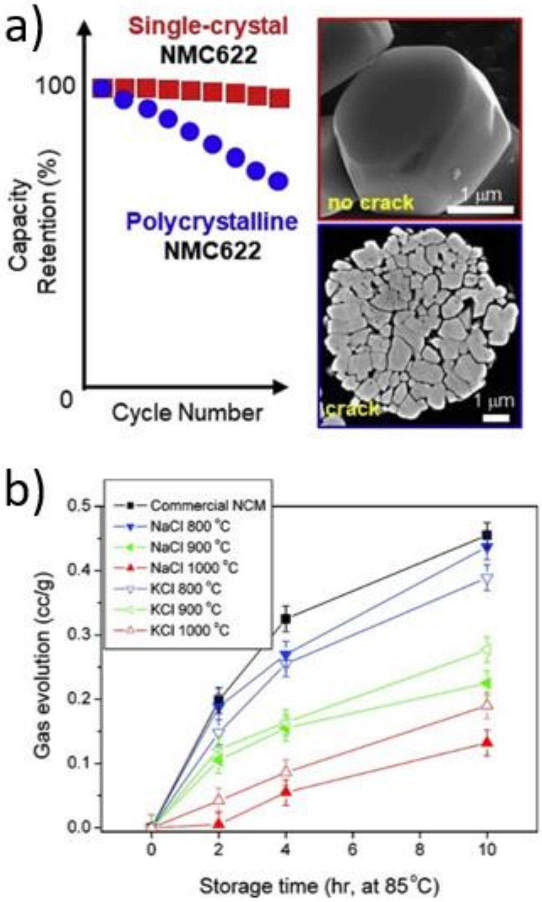

Figure 3. a) Cyclic performance and SEM image of single crystal and polycrystalline NMC cathodes after 300 cycles. Reprinted from Energy Storage Materials, Vol 27, Qian, Zhang, Li, Zhang, Xu, Cheng, Xie, Wang, Rao, He, Shen, Chen, Tang, Ma, Single-crystal nickel-rich layered-oxide battery cathode materials: synthesis, electrochemistry, and intra-granular fracture, 140-149., Copyright (2020), with permission from Elsevier. b) Evolution of gas (cc/gram of NCM) from charged electrodes (4.45 V) with respect to storage time at 85 ˚C. Reprinted with permission from (Y. Kim, ACS Applied Materials & Interfaces 4, 2329. Copyright (2012) American Chemical Society.

The random crystal orientation in polycrystalline assemblies results in anisotropic volume changes on charging. The absence of such stresses in single crystal materials may therefore reduce the likelihood of inter-granular fracture (**Figure 3a**). Considering the nickel-rich material $LiNi_{0.83}Co_{0.11}Mn_{0.06}O_2$, single crystal morphologies have shown excellent long duration cycling performance and thermal stability in half cells at 25 and 55°C and full cells at 45°C.[31] These observations are in addition to reduced Ni migration to the anode observed for single crystal NMC811, when compared to polycrystal NMC811.[32] However, intra-granular fracture is not entirely mitigated, and does still occur when single crystal NMC particles are severely overcharged (e.g. to 4.7 V, >0.84 Li^+ extraction per NMC).[27]

Morphology may also play a role in suppressing gas evolution through a reduction in electrolyte side reactions, a concern around safe battery operation and storage. **Figure**

3b evaluates the influence of morphology on gas evolution when storing NMC811 single crystal particles obtained through flux synthesis at different states of charge. The reduced gas evolution correlates to the reduced surface area in the single crystal materials, since there are no internal pores and intergranular boundaries along the surface.[30] Micro-cracking has also been observed for single crystal Ni rich cathodes through plane gliding on charge which is reversed on discharge.[33] Despite increased performance, synthetic challenges have limited the reports on single crystal materials to date.[34,35] However, the development of new synthetic approaches to single-crystal nickel-rich cathode materials could improve energy density, safety and durability in lithium-ion batteries.[36]

Concluding remarks

Owing to their successful history as cathodes, layered oxide materials remain the current cathode of choice for lithium ion batteries, especially for automotive applications, with some low-cobalt and high-nickel compositions already primed for commercialisation. To fully reap the benefits of these, efforts to mitigate and overcome deleterious degradation processes that impair such nickel rich compositions are essential. Strategies involving the introduction of electrochemically inactive, stabilising cations into the structure and applying stable surface coatings have proved successful in prolonging the cycle life. A synergistic approach involving doping, coating and sophisticated particle engineering is an attractive route for the cathodes of the future.

3. High Voltage through Spinel Materials

Beth Murdock, Li Zhang and Nuria Tapia-Ruiz

As discussed, the demand for high-energy density lithium ion batteries has driven cathode research toward developing materials with increasing storage capacity (> 200 mAh g^{-1}) and operating voltage (> 4.0 V vs. Li^+/Li). High-voltage spinel materials, with general formula $LiMn_{2-x}M_xO_4$ (M= Co, Cr, Fe, Cu and Ni), have emerged as promising materials to meet future energy density requirements due to their high working voltages around 5 V vs. Li^+/Li.[37] Among these, the $LiNi_{0.5}Mn_{1.5}O_4$ (LNMO) spinel has shown great promise owing to its high energy density (650 Wh kg^{-1}) provided by the two-electron $Ni^{2+/4+}$ redox couple operating at high voltage (≈ 4.7 V vs. Li^+/Li), superior rate capability, and thermal stability.[38] Furthermore, LNMO offers a Co-free and therefore, safe, cost-effective and sustainable alternative to $LiCoO_2$ and NMC-type commercial materials, which provide lower energy densities (518 and 576 Wh kg^{-1}, respectively).

LNMO can crystallise into two cubic structures; the ordered ($P4_332$ space group) and disordered (Fd-3m space group) phases, that differ on the site location of the Ni^{2+} and Mn^{4+} ions within the crystal lattice (**Figure 4a**).[39] The disordered phase is obtained at temperatures above 700 °C, causing oxygen loss and the reduction of Mn^{4+} to Mn^{3+} ions, leading to a random distribution of the Ni and Mn cations over the 16d sites. Such oxygen vacancies also encourage the formation of a secondary rocksalt phase ($Li_{1-x}Ni_xO$) resulting in the presence of both this nickel rich impurity and Mn^{3+} ions in samples that are fast cooled from 900°C. Slow cooling, on the other hand, can effectively allow the dissolution of the rocksalt phase. Such cooling is insufficient, however, for instigating long-range order, in which the Ni^{2+} and Mn^{4+} ions occupy the 4a and 12d sites, respectively. For such conversion, long annealing, at temperatures between 600 - 700 °C, is required.[40]

Clarity as to how ordering affects the electrochemical performance is not offered within the literature, with contrasting opinions presented throughout. The presence of increased impurity phase within disordered samples, compared to ordered samples, makes attributing any changes in performance to differences in long-range order difficult.[40] The disordering of the Ni^{2+}/Mn^{4+} ions and presence of oxygen vacancies (and Mn^{3+} ions) often results in superior performance compared to the ordered phase in terms of cyclability and rate performance.[41] The enhanced cycling stability is attributed to a reduction in lattice strain of the (de)lithiated products, leading to a more solid-solution-like behaviour (**Figure 4b**); whereas the oxygen vacancies and Mn^{3+} ions are responsible for the improved Li-ion and electron mobility.[40] Micron-sized, ordered LNMO particles have shown impressive cyclability and high rate capability, suggesting that long-range ordering may not be a limiting factor.[42] Neutron pair distribution function (PDF) has shown identical local environments in both ordered ($P4_332$) and disordered ($Fd\text{-}3m$) LNMO samples below 5 Å, and a *partially*-ordered region up to 16 Å for the disordered LNMO sample, demonstrating that the disordered sample is comprised of Ni/Mn ordered and semi-ordered nano-domains. It is therefore suggested that long-range order may not have such a profound effect on the electrochemical performance but instead the ordered domain size and boundaries may be more influential.[43]

Despite its great promise, there are still critical barriers to overcome for the commercialisation of LNMO materials, including synthetic challenges, bulk and surface instabilities at high states of charge and the absence of compatible high-voltage electrolytes. All these factors contribute to the poor initial coulombic efficiency, capacity decay and subsequently increased cell impedance, especially at moderate temperatures and when used in full-cells with a graphite anode.

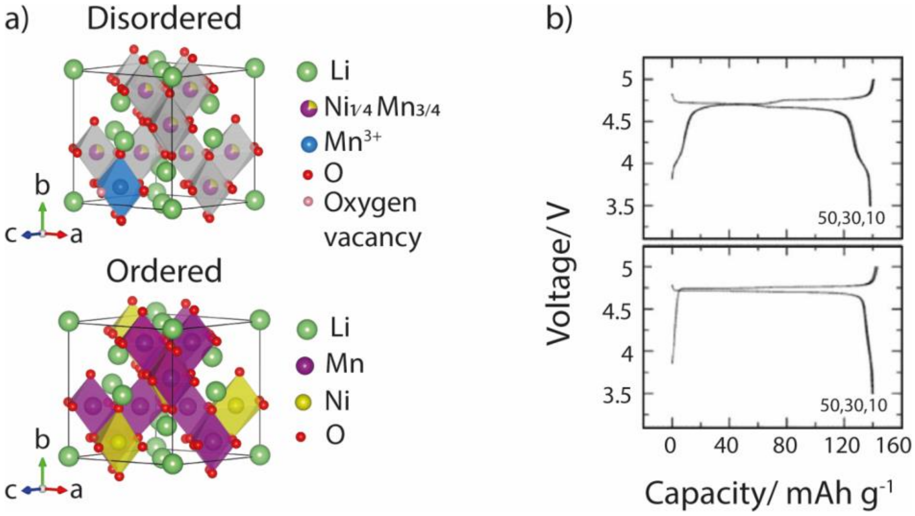

Figure 4. a) Schematic structures of ordered and disordered LNMO materials.
b) Charge/discharge curves of disordered (top) and ordered (bottom) LNMO at C/7 (20 mA

g^{-1}). Figure b) is reprinted with permission from (J.-H. Kim, S.-T. Myung, C.S. Yoon, S.G. Kang, and Y.-K. Sun, Chemistry of Materials 16, 906. Copyright (2004) American Chemical Society.

Spinel-type materials suffer from bulk and surface instabilities at high charge states, where their full capacity is attained. Here, competing reactions involving electrolyte decomposition of both solvent and salt take place. This occurs due to the anodic instability of commercial carbonate-based electrolytes above 4.5 V vs. Li^+/Li.[44] The inorganic $LiPF_6$ salt decomposes into PF_5 and LiF, with the former further reacting with traces of water to form HF and POF_3 species.[45] On the other hand, the organic carbonate-based solvent reacts at the surface of LNMO to form a variety of organic compounds, e.g. species with carbonyl groups, oligomers and alkyl carbonates.[46]

The oxidative decomposition of the electrolyte has shown to corrode the cell components[47] and, more importantly, leads to the rapid self-discharge of LNMO by inserting Li^+ ions from the electrolyte into the structure while reducing Mn^{4+} and Ni^{3+}/Ni^{4+} ions.[48] Subsequently, disproportionation reactions of the type $2\ Mn^{3+} \rightarrow Mn^{4+} + Mn^{2+}$ occur, leading to the formation (and posterior dissolution) of Mn^{2+} ions.[49] This degradation mechanism is well known for $LiMn_2O_4$ cathodes [50] and in LNMOs is particularly critical in full-cells, given the limited Li supply.[51] Dissolved Mn^{2+} ions not only translate into active material loss but also trigger the migration of Mn ions into empty tetrahedral Li sites at high states of charge to form the Mn_3O_4 spinel phase on the surface of LNMO, which is also soluble in the electrolyte.[52] Furthermore, transition metal (TM) migration to empty octahedral sites at subsurface regions leads to the formation of rocksalt-like structures with subsequent oxygen evolution (**Figure 5**).[52]

O_2, together with CO and CO_2 evolved from the decomposition of the organic solvent,[46] contribute to the swelling and ultimate failure of the cell.[53] Additionally, CO_2 can be reduced at the anode by reacting with Li to form Li_2CO_3, aggravating the capacity decay.[54] TM dissolution occurs independent of the Ni/Mn site order and it is highly dependent on several factors such as temperature, storage time and state of charge.[49] Ni and Mn dissolution lead to the formation of LiF, MnF_2, NiF_2 and polymerised species on the cathode surface, increasing the cell impedance.[49] At the anode surface, on the other hand, dissolved Mn and Ni ions are reduced to form Mn and Ni particles while obstructing the diffusion of Li^+ ions into the structure, promoting the formation of a thick solid-electrolyte interface (SEI) layer.[49]

Finally, optimisation of the synthesis methodology by controlling the level of Ni/Mn disorder and the amount of redox-inactive rocksalt $Li_xNi_{1-x}O$-like impurity is necessary given their strong correlation with the electrochemical performance.[55]

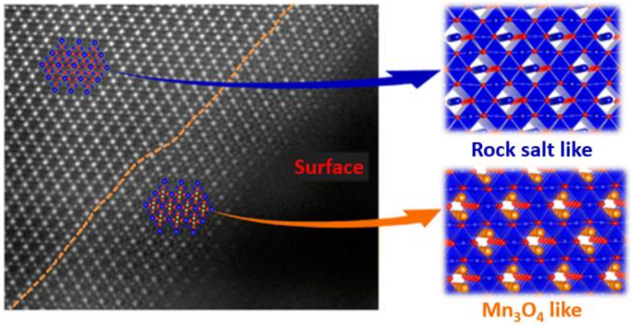

Figure 5. Schematic representation showing the structural complexity of LNMO. HRTEM studies show that during cycling between 3.5 and 4.9 V a Mn_3O_4-like phase forms on the surface of LNMO together with a rocksalt-like phase on the subsurface. Reprinted with permission from (M. Lin, L. Ben, Y. Sun, H. Wang, Z. Yang, L. Gu, X. Yu, X.-Q. Yang, H. Zhao, R. Yu, M. Armand, and X. Huang, Chemistry of Materials 27, 292). Copyright (2014) American Chemical Society.

Advances related to bulk and surface structure control and electrode/electrolyte stabilisation are needed for high-voltage spinels to expand their presence in the lithium-ion battery market. Numerous reports have been published on the use of doping strategies to improve the electrochemical performance of LNMO.[56,57] Elemental doping effectively solves the formation of rocksalt phases during synthesis, improving the overall cycling performance.[57] Furthermore, the site location of these dopants has a direct effect on the properties of LNMO. For example, dopants located on the Li 8a site, such as Na^+[58] and Ti^{4+},[59] improve the charge transfer and, more importantly, alleviate the problem on TM dissolution. On the other hand, dopants on the 16d octahedral sites, such as Fe^{3+}, Cr^{3+}, Co^{3+}, Al^{3+}, Cu^{2+} and Mg^{2+}, enhance the electronic conductivity as well as thermal and structural stability of LNMO.[57,60] Oxygen substitution with more electronegative anions, e.g. F^- ions, has been shown to minimise TM dissolution during cycling due to structure stabilisation.[61]

The modification of the surface properties in LNMO has been shown to also stabilise the LNMO/electrolyte interface. Several works have described the importance of surface orientation, showing strict correlation between this parameter and the electrochemical performance observed in the LNMO particles studied.[62] Furthermore, surface-doping has been claimed to be more effective than bulk-doping to alleviate TM dissolution. In $LiNi_{0.5}Mn_{1.2}Ti_{0.3}O_4$, the formation of a titanium-oxygen-enriched cathode electrolyte interface (CEI) layer plays an important role in stabilizing the surface of LNMO.[63] Surface coatings may also provide a more stable electrode/electrolyte interface by minimising TM dissolution, electrolyte oxidation and other side reactions. These include: (1) electronic-conductive coatings, which improve the charge-transfer kinetics of LNMO, particularly at high rates (e.g. carbon coatings,[64] polymer coatings;[65] (2) ionic-conductive coatings that allow for superior Li^+ ion diffusion through the use of Li^+ ion conductive materials (e.g. Li_3PO_4,[66] $Li_4P_2O_7$[67] and Li_2SO_3,[68]); and (3) acid-protective coatings that aim to defend against HF corrosion of the LNMO cathode (e.g. SiO_2,[69] TiO_2,[59] Al_2O_3).[70] Hybrid coatings provide a combination of the afore-mentioned advantages. For example, Li_3PO_4-TiO_2 shows the hybridisation of an ionic- and electronic- conductive coating, providing enhanced ionic and electronic conduction as well as minimising TM dissolution.[71]

Aside from the optimisation of LNMO materials and their interface, a major leap forward in this technology will occur after developing suitable and safe electrolyte formulations with high anodic stability that form a stable SEI layer on the anode. To date, literature reports have focused on modifying the current state-of-the-art electrolytes by adding additives[72] or sacrificial salts[73] that provide a stable CEI layer by becoming oxidised at the cathode surface prior to the electrolyte. Furthermore, novel liquid solvents such as ionic liquids,[48] sulfone-[74] and nitrile-based[75] and solid-electrolytes[76] have been considered. Concentrated electrolytes, such as concentrated LiFSA/carbonate ester mixtures,[77] are gaining attention due to their unique solvation chemistry in which anions take precedence over solvent molecules. This allows greater flexibility in solvent choice, opening possibilities for solvents previously disregarded. Nevertheless, these electrolytes are still far from providing LNMO with optimal battery performance and, thus, require further refining.[78]

Concluding remarks

High-voltage spinels are a promising high-energy density cathode alternative to be used in future EVs and HEVs. To date, the lack of in-depth studies on high-voltage advanced electrolytes has driven research toward solving issues related to the stabilisation of the cathode (bulk and surface) and electrolyte, as well as their interphase. These issues directly compromise the long-term cycling performance of LNMO/graphite full-cells at moderate temperatures (i.e. in “real” conditions), preventing their use in future applications.

Multiple strategies such as elemental substitution, surface engineering and the use of electrolyte additives, among others, have proved successful in improving the cycling stability in full-cells. It is anticipated that a combination of these strategies will lead to further improvement in performance. Furthermore, a better understanding of the surface degradation reactions and their dependence on the cathode and the anode choice must be sought to minimise capacity decay. Finally, corrosion of cell components and their effects on electrochemical performance represents an understudied research area which will require further attention.

4. High Capacity through Disordered Rocksalts

Kirstie McCombie, Xuan Zhi, Edmund J. Cussen and Anthony R. West

Disordered rocksalt (DRX) materials have only relatively recently been considered as potential cathodes. These materials offer the possibility of significant increases in capacity (>300 mA h g^{-1}), operation at high voltages, and high energy densities up to 1000 W h kg^{-1}.[79] These materials are classified by a disordered arrangement of Li and transition metal atoms on the same cation sites within an α-$LiFeO_2$ structure. Many studies on ordered layered rocksalt materials followed the commercial introduction of $LiCoO_2$, with particular attention to the factors that control Li diffusion kinetics.[80,81] The energy barriers for Li hopping were found to increase significantly in the presence of disorder and, including the effects of channel blocking, lead to loss of performance and reduced cyclability. However, a report of high specific capacity, 253 mAh g^{-1}, combined with good cyclability in the disordered rocksalt Li_2VO_3,[82] led to a re-examination of the effects of cation disorder. Similarly, $Li_{1.211}Mo_{0.467}Cr_{0.3}O_2$, has shown good reversible cycling behaviour, providing 265 mAh g^{-1} capacity, despite transforming to an apparently disordered rocksalt after 10 cycles. The broad accessibility of these materials is demonstrated by examples such as the cation-disordered rocksalts, $Li_{1.3}Nb_{0.3}M_{0.4}O_2$ (M=Mn, Fe, Co and Ni) which showed facile Li migration through a percolation network and large reversible capacity.[83]

When looking at the development of such materials, the abundance, broad geographical availability and low cost of manganese combine to make Mn-based disordered rocksalts highly attractive targets as cathode materials. The high capacity offered by these materials has been shown in a number of example studies, to originate from a combination of both cation and anion redox contributions. In the disordered $Li_4Mn_2O_5$ structure for instance, the initial capacity of 355 mA h g^{-1} is far higher than the theoretical capacity from the transition metal redox contribution alone which would be 245 mAh g^{-1} (Mn^{3+}/Mn^{4+} and Mn^{4+}/Mn^{5+}). X-ray absorption spectroscopy (XAS) and resonant inelastic X-ray scattering (RIXS) measurements have demonstrated the significant oxygen redox contribution of these materials.[84-87] The activation of oxygen redox presents both an opportunity and a challenge in the area of cathode materials. Established materials such as $LiCoO_2$ and $LiFePO_4$ use localised oxidation of Co^{3+} and Fe^{2+}, respectively to permit de-intercalation of Li^+. In these classic examples, the role of the oxide or phosphate sublattice is to provide a passive framework that largely retains the Li^+ sites as vacancies which are well-matched for Li^+ re-insertion during battery cycling. The presence of oxide redox enhances capacity, but at the cost of activating the chemical reactivity of oxide ions. Many of the challenges, and opportunities, associated with disordered rocksalts arise from understanding, limiting and controlling the oxygen redox contribution.

Inducing cation disorder within a material can pose significant experimental challenges. One approach, high energy ball milling can transform ordered monoclinic Li_2MnO_3 into a disordered rocksalt structure that shows a reversible capacity of 250 mAh g^{-1} at 3 V (**Figure 6a**).[88] The nature of the disorder in this phase continues to attract scrutiny and recent reports showed that, although the average structure of nanosized Li_2MnO_3 is cubic, the local structure is composed of short-range ordered layers (**Figure 6b**).[89] The short range ordering in these materials has a deleterious impact on the performance of the cathode; mitigation approaches include attention to material compositional design as well as an improved synthetic pathway.[86,90]

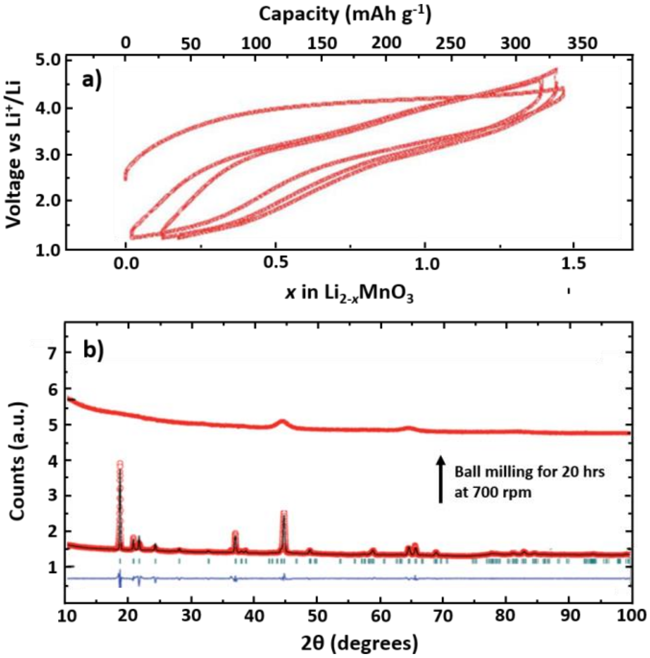

Figure 6. a) Galvanostatic charge/discharge data obtained for Li_2MnO_3 at a rate of 1 Li^+ per formula unit in 20 hours (11.5 mAh g^{-1}) cycling to 4.4 V, 4.6 V and 4.8 V on the first 3 cycles. b) The powder X-ray diffraction pattern obtained for Li_2MnO_3 as prepared by the solid state reaction after 20 hours of highly energetic ball milling. Reproduced from Ref. 88 from The Royal Society of Chemistry under Creative Commons Attribution CC BY 4.0.

There appear to be at least three routes to synthesis of disordered rocksalt structures. The first is via ball milling ordered structures of the same composition, such as has been achieved with Li_2MnO_3. The second is by rapid quenching from above the temperature of the order-disorder transition so as to preserve the disordered material at ambient temperature, as achieved with $Li_{1.25}Nb_{0.25}Mn_{0.5}O_2$.[90] The third, and most widely applicable method, uses mechanochemical activation in which, following Ostwald's law of successive reactions, the first product is frequently entropy-stabilised and either fully or partially disordered, but metastable; kinetic stability of the product is obviously essential to its usefulness. This method offers great scope for compositional tuning to optimise properties, whilst keeping a watchful eye on product stability.

To achieve both high capacity and high cycling stability, it is necessary to activate the oxygen redox, but limit the scope for further oxidation to form molecular O_2, which can escape the lattice leading to irreversibility and loss of capacity. Considered at the battery level, O_{-2} loss presents the risk of gas evolution with associated mechanical, containment and safety problems.

The stabilisation of disordered rocksalt structures by d^0 transition metal cations is, in part, due to their ability to accommodate large octahedral distortions with a low energy cost due to the absence of crystal field splitting energy. The presence of d^0 elements in the structure has been proposed to minimise oxygen redox processes and a large majority of disordered rocksalts reported to date contain d^0 dopants, most commonly Ti^{4+}, V^{5+}, Nb^{5+}, and Mo^{6+}.[79] A possible cause of enhanced cycling stability comes from the ability of the d^0

cations to coordinate various, partially-oxidised oxygen anions. Examination of the related compositions $Li_{4+x}Ni_{1-x}WO_6$ showed that the presence of reversible oxygen redox was facilitated by coordination of the peroxo species $(O_2)^{2-}$ to the W^{6+}, d^0 cation.[91]

The substitution of Mn by various transition metals has been screened using density functional theory.[92] From the results, niobium was selected as the best dopant giving superior properties compared to 3d dopants. The authors successfully prepared phase-pure $Li_{1.95}Mn_{0.95}Nb_{0.05}O_3$ and demonstrated that Nb doping increased the reversible capacity while also impeding decay of the discharge potential.

A major challenge is to find suitable preparative routes to deliver materials that combine reversible oxygen redox and associated additional capacity compared with that obtained from Mn redox activity alone. As a note of caution, high capacity has also been observed where the introduction of excess lithium led to formation of a composite whose high capacity was delivered by the presence of Li_2O, trapped in vacancy clusters on the cathode surface.[93] Such extrinsic capacity may be useful, but careful characterisation is vital to avoid pitfalls of mis-assigning capacity to targeted phases where an impurity or undetected secondary phase is responsible.

One route to combine oxygen and transition metal redox is to manipulate the latter via judicious doping of the anion lattice. Li_2VO_2F prepared by ball-milling shows the disordered oxyfluoride can deliver a higher capacity than the analogous oxide Li_2VO_3.[94] Significantly, the lithium content and fluorine content of the DRX structure should not be considered in isolation.[95]

Whilst high energy ball milling has long been used to reduce particle sizes and achieve intimate mixing of reagents, direct mechanochemical synthesis has only recently become established as a versatile new synthetic method, especially suited to synthesis of new, redox-active cathode materials. However, better understanding of the milling conditions, choice of reagents and control of atmosphere is still needed, together with the factors that control compositional extent of single-phase products, their defect structure and kinetic stability.

The concept of redox-active oxygen in solid state materials appears to have been accepted with considerable reluctance by the chemical community but given its unavoidability in accounting for the very high reversible capacities of some cathodes, it is clear that new opportunities exist to build on these discoveries. However, better understanding is needed of the compositional or structural parameters that favour oxygen redox, whether the holes that are generated on charging are small polarons located on either individual oxygens, short chain catenated peroxo species or large polarons associated with transition metal *d* – oxygen 2p hybridised orbitals and band structure. The need to limit oxidation to one electron per oxide ion is referred to above.

Control of transition metal oxidation states by aliovalent cation doping is a very well-established doping strategy. Aliovalent anion doping, with replacement of O^{2-} by halide$^-$ or N^{3-} ions is much less well investigated, but has already achieved considerable success, as shown by synthesis of Li_2MnO_2F, and has much scope for further development.

The role of disorder in structures is complex with highly disordered phases showing unexpected high Li^+ conductivity and high capacity. Further, by careful choice of material processing condition, it is possible to control both the size of the disordered rocksalt particles and the domain size of ordered regions within rocksalt sublattice. The role of simulation and experimental probes below the Bragg diffraction limit (total scattering PDF analysis, NMR, EXAFS, simulation) are essential for an improved understanding of the effect of these different length scales on resulting electrochemical properties.

Concluding remarks

The capacity of disordered rocksalts can greatly exceed that of current commercial cathodes. The potential capacity of 460 mA h g^{-1}, realised in Li_2VO_2F, offers the promise of energy densities exceeding 1000 mA h g^{-1} that could double the energy stored in commercial batteries.[96] Achieving this performance safely over the lifetime of a commercially viable battery is the key challenge and kinetically limiting the oxygen redox is likely to be an important strategy in addition to thermodynamic control. Significant opportunities for improvement are provided by the range of cation and anion dopants that can be introduced into the structure. In addition to using classic solid state approach of aliovalent cation dopants to manipulate charge balance, it will also be necessary to incorporate knowledge from coordination chemistry to consider bonding to partially oxidised oxygen species and help stabilise the oxygen redox.[91] Many of the above factors attest to the importance of both cation and anion disorder within the rocksalt crystal structure. We are fortunate that these discoveries are proceeding in tandem with major advances in our understanding of local structure, through advanced experimental techniques and modelling capabilities.

5. Sustainable Alternative Chemistries

Viktoria Falkowski, Xabier Martínez De Irujo Labalde, Michael A. Hayward and Simon J. Clarke

Committing to sustainability, the requirements for current cathode research extend beyond the development of cheaper, lighter, and safer cathodes with superior electrochemical performance. Important aspects like low-energy synthesis routes and the use of earth-abundant, non-toxic and recyclable materials are increasingly coming into focus.

The $LiCoO_2$/C cell technology still provides the backbone of cathode research, however, due to the issues implied with this system, the emphasis of recent efforts has been on non-traditional electrode materials complying with sustainability demands. Especially, compounds displaying reaction mechanisms that diverge from conventional intercalation-based cathodes, that exclusively rely on the electrochemistry of their redox-active TM cation centers, e.g. the redox couple Co^{3+}/Co^{4+} in LCO, have attracted attention. The additional utilisation of anion redox mechanisms in cathode materials provides higher capacities, given that more Li can be removed and inserted per formula unit of cathode material. Here, the anions (mostly oxygen) also participate in redox processes by forming dimers of the anion species like the oxo- (O^{2-}) to peroxo-like $(O_2)^{n-}$ transformation observed in Li_2IrO_3 or in $Li_2Ru_{1-x}Sn_xO_3$ or the (S^{2-}) oxidation to $(S_2)^{2-}$ in Li_2FeS_2 upon cycling.[97-102]

Compounds that exhibit reversible conversion reactions with lithium have also been considered as another interesting alternative, offering higher theoretical capacities than intercalation-based systems. Unlike intercalation, conversion based lithiation/delithiation involves complete structural disintegration and rearrangement, passes through several intermediate phases and can be expressed as $TM_xX_y + zLi \rightleftarrows xTM^0 + yLi_{(z/y)}X$ or $zLi + X \rightleftarrows Li_zX$, where Li = lithium, TM = transition metal, X = anionic species.[103,104] Transition metal fluorides are regarded as the most promising conversion materials as they offer good operating voltages e.g. 3.55 V vs Li/Li^+ in CuF_2 and high gravimetric capacity as found for FeF_3 (712 mAh g^{-1}).[105,106] Lithium-Chalcogen reactions are also considered as conversion systems and can be described as $zLi + X \rightleftarrows Li_zX$. Based on naturally abundant, low-cost and environmentally benign resources, LiS and LiO_2 with their high theoretical capacities (1166 mAh g^{-1} and 1168 mAh g^{-1}) and potentials (2.28 V and 2.96 V vs Li/Li^+), are the most promising candidates for chalcogen-based conversion cathodes.[107,108] Recently another material class showed conversion-type electrochemical reactions with lithium. Transition metal carbodiimides such as FeNCN show good cycling properties and excellent capacity retention.[109,110]

These promising materials and concepts display the potential that arises through expansion of the chemical systems under investigation and going beyond traditional cathode chemistry.

As promising as these new cathode systems seem, they still have some challenges to overcome to be considered suitable to industry. These materials have to meet many demands:- hinging on redox-active elements with high elemental abundance, offering high performance, good cyclability, low cost, low volume expansion and their synthesis should be scalable and, at best, environmentally friendly.

A major challenge of oxide-based electrode materials utilizing anionic redox is the loss of oxygen from the structure at high potentials caused by the irreversible formation of O_2, as with the DRX materials described previously. The evolution of the volatile component leads to structural degradation of the cathode, electrolyte oxidation and can cause a thermal runaway and the release of toxic and flammable compounds.[111-113] In the case of sulfide cathode materials the anionic redox is more reversible, but as a trade-off limits the voltage.[114]

Conversion processes with materials like FeF_3 and CuF_2 can offer vast capacities, however their reactions involve complete structural disintegration and rearrangement during cycling, which can result in volume changes and active material loss through incomplete conversion reactions. While metal halogen bonding in metal halide cathodes enables the significant increase of the working potential, the ionicity of these bonds results in poor electrical conductivity.[115,13,116]

An in depth understanding of the challenges present in these different systems, and optimising methods to overcome these, is fundamental to the design of new cathode materials. The steps involved between the theoretical concept, synthetic realisation and optimisation at a lab scale, and routes towards its industrial implementation are vast and complex as represented within this work and in the scale of the wider field.

With an idea of how the desired product should look like, the realisation may involve sophisticated multistep-approaches to yield the desired structure or control the oxidation state of specific elements. For example, the layered modification of $LiMnO_2$ could not be obtained by direct synthesis routes, but it was possible by a cation-exchange reaction in previously synthesised layered $NaMnO_2$.[117]

When moving from research stage studies to considerations of introducing new compounds as cathodes, the cost and abundance of the raw materials and the feasibility of scale-up play an important role. Also, the geopolitical concentration of elements is not to be neglected, especially if there is a global dependence on the supply from one or a few countries. Conventional cobalt containing cathodes suffer from comparably low abundance, high costs and the reliance on supplies from the Democratic Republic of Congo associated with the element. Recycling is unlikely to provide significant short-term supply, hence fostering the search for and in-depth investigations of Co-free alternatives. On the other hand, the supply of the inexpensive elements including Fe, Mn, Ni, O, F, and S can meet the future demands, thus cathodes mainly consisting of such abundant elements are coming increasingly into focus.[118,119]

Research-laboratory synthesis usually yields materials in small quantities and with minimal restrictions in terms of synthetic methods. Due to possible variability in the compounds when prepared in large batches, and morphological optimisation are crucial considerations as even the most promising material cannot be used commercially if high-volume manufacturing is not possible or too costly. This relates directly to the $/kWh metric examined earlier.

Structural degradation is an issue that all electrode materials face over time. But with studies that reveal its causes and provide new insights into why some materials exhibit superior structural integrity and reversibility, the first life performance of electrode materials is continually improving.

Great advances have been achieved to overcome the irreversible O_2 release after anion redox, when the battery is operating at the desired high voltages. As indicated with the DRX materials, stabilisation of the oxide can be achieved by suppressing the anion-transition metal charge transfer by adding d^0 elements in the cation sublattice (i.e. Ti^{4+}, Nb^{5+} or Ta^{5+}) or the substitution of O^{2-} by F^- within the anion sublattice.[120,121] Furthermore, there is evidence that the different intermediate oxygen species, such as the peroxides and superoxides, are stabilised at high voltages without O_2 evolution in some 4d and 5d transition metal oxides.[98-100] Such results are encouraging when looking to exploit anion redox processes. However, the cost and additional mass of 4d and 5d elements make them unattractive as the main components in a cathode material. Mixed anion systems are also highly suited to stabilise the anionic redox and maintain high working potentials. Oxysulfides like the anti-perovskite material Li_2FeSO show promising behaviour. In this material Fe shows redox activity at low states of charge, whereas at higher states of charge the sulfur is responsible for the redox reaction, with oxygen remaining as O^{2-} during cycling.[122-124] Even if this class of material exhibits lower voltages than pure oxide-based cathodes, the advantage of such low-cost and environmentally friendly compounds, offering longer life spans of batteries cannot be ignored.

The high energy consumption that is often associated with the preparation of current state-of-the-art cathode materials is another main issue which cannot be neglected, especially when thinking about the additional demand associated with conversion from conventional fuels to electric vehicles. Using low-temperature processes, such as hydrothermal synthesis and multistep approaches like ion-exchange, can open the doors to a more sustainable era. Beyond that, the use of multistep synthesis can give us access to an assorted range of new materials even out of the thermodynamic equilibrium with a tailored control of the crystal and electronic structure. For instance, within the $LiFeO_2$ composition, topochemical manipulation triggers the formation of metastable structures with an enhanced cyclability in comparison with the most stable disordered material obtained by the conventional ceramic route.[125,126] Aside from the crystal structure tailoring, topochemical methods allow transition metal oxidation states to be controlled, which could be a promising tool for the next generation of cathodes. In particular, avant-garde post-synthetic topotactical reduction processes could put novel redox pairs into play by stabilising unusual low oxidation states such as Ni^+ in $LaNiO_2$ to tune the corresponding electrochemical window.[127] These developments also contribute to the realisation of the scale-up of materials which could not be obtained cost effectively and in a high volume so far, making them more commercially attractive.

Precise manipulation of the materials offered by these novel approaches can also be complemented by the multiple possibilities of additional computational input. *Ab initio* calculations can support synthetic approaches by identifying new stable compositions and predicting their crystal structure, as detailed in the following section.

Concluding remarks

The exploration of alternative cathode chemistries offers major benefits going beyond sustainability and lowering the production cost. By expanding the field of material classes considered as potential electrode materials, we see and learn from unique features in their (de)lithiation processes that occur during battery cycling. These insights, which can be supported by additional computational input, can finally guide the development of better cathode materials in general. As we move away from traditional battery materials, however, we recognise the need to make advances in the synthetic approaches used, as the preparation of such materials is often challenging, and structural optimisation is required to fully exploit the potential of these structures.

6. Searching for New Materials through Crystal Structure Prediction

Bonan Zhu, Ziheng Lu, Chris J. Pickard and David O. Scanlon

The elemental composition of cathodes is critical to the overall performance of lithium-ion batteries (LIB). The history of cathode development shows that advances in performance have been fueled by the experimental discovery of new materials or material systems.[128]

There are many possible selection criteria for cathode materials. Key among them are the energy density, reliant on the amount of Li available for cycling and the average working voltage, and the rate capability which is limited by the Li diffusion barrier within the material. The widespread utilisation of first-principles methods, in particular density functional theory (DFT) calculations,[129] combined with ever-increasing computing power have allowed computational chemists to study these systems at the atomistic level and give an accurate explanation of the mechanisms behind the performance-critical processes such as charge transfer, lithium diffusion, and phase transition. In a complementary manner, the atomic structure of the underlying material is an essential input for computational studies, which are typically obtained experimentally via characterisation techniques such as powder X-ray/neutron diffraction and electron microscopy. This is, of course, only possible if the materials have already been synthesised.

Methods of first-principles crystal structure prediction have been developed to allow prediction of the structure of unknown materials with little or no experimental data. They have been applied to a wide range of fields,[130] but represent a virtually untouched frontier for cathode materials. A few studies successfully reproduced experimentally known phases of cathode materials.[131,132] We have excluded the discussion of species-substitution based approaches[133] as they are interpolative and dependent on the underlying databases and therefore bias towards currently known phases. This limits their applicability in unexplored regions of the composition and phase spaces.

Structure prediction is typically based on basin/minima hopping,[134,135] genetic algorithms,[136] particles swarm optimisation,[137] and random searching,[138,139] with the last being our choice for the FutureCat project. The *ab initio* random structure searching (AIRSS) approach[138,139] a straightforward method that explores the distribution of basins of the potential energy surface (PES) by generating random “sensible” structures based on sound physical and chemical considerations, such as the number density of atoms, species-wise separations, and space group symmetries. Making no attempt to *learn* the PES, the search is insensitive to the precision and accuracy of the underlying energy evaluations (eg. DFT calculations) and can be trivially parallelised. Symmetries can be exploited to gain further speedups in DFT calculations by several folds, and the reduction in the degrees of freedom will further accelerate the convergence of the local relaxations. Accurate, but costly, calculations, possibly involving high levels of theories, only need to be performed for a small number of selected low-energy structures. In addition, very often it is not only the ground state structure that is of interest, but also metastable polymorphs, which are also encountered in the search. Results of exploratory searches can be used to provide guidance for experimental works. In fact, the AIRSS method can be interpreted as a *computational synthesis* of materials, in that the generated random structures resemble those at extremely high temperatures, i.e. the atoms are extremely energetic and are well-mixed. Therefore, an AIRSS search is similar to an experimental trial to synthesise a material by quenching (relaxing) it after heating at extremely high temperatures (which results in randomly generated structures), as illustrated in **Figure 7**. Given enough trials, one can find a structure that is thermodynamically stable. On the other hand, searching can be tailored based on existing experimental findings, and support cases where the atomic structures are only partially resolved.[140]

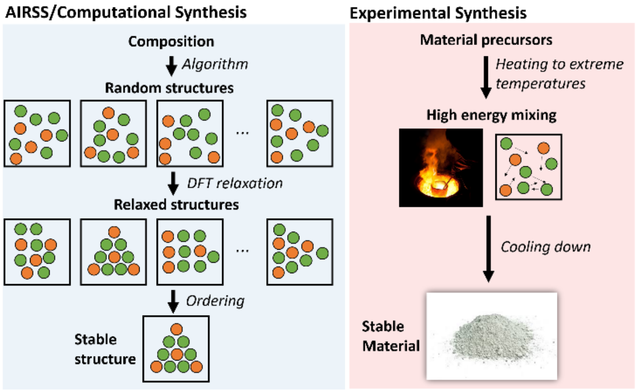

Figure 7. Comparison between an AIRSS search of a composition and an experimental synthesis of a material.

Transition metal (TM) intercalation cathodes typically contain three or more elements: Li, TM ions and anions, and there can be four or more elements for polyanion-based materials as well as those with mixed cation/anions. The complexity of the PES increases with the number of elements under consideration. Magnetism, originating from the transition metal ions, also poses additional challenges as the degrees of freedom in spin induce additional local minima on the PES. Unlike atomic positions, the electronic spins are not fully controllable in the calculations. Hence the PES can be ill-defined, as multiple solutions of the electronic structure become possible for a given structure. Fortunately, it may be sensible to decouple the spin and positions, since quite often the energy differences between various spin configurations are relatively small. Standard DFT calculations usually give poor descriptions of transition metals due to the self-interaction error associated with localised electrons. A popular approach to address this is to apply the +U correction,[141] but it should be noted that the value of the U has to be chosen carefully. An alternative approach is to use hybrid functionals such as HSE06,[142] however this leads to orders of magnitude increases in the computational cost.

Another shortcoming of crystal structure prediction is that, as the name suggests, it only considers crystalline solutions. The existence of a periodic solution does not always mean the material will be crystalline. On the other hand, a random search does produce disordered-like structures at higher energies, although the unit cells are relatively small. In reality, many cathode materials exhibit certain degrees of site-occupancy disordering, such as the disordered rocksalt materials.[79] The ensemble of the produced structures may give clues about the ordered/disordered nature of the target material. The role of disorder in cathode structures is examined in detail in section 10ii.

The vast size of the chemical space poses another challenge for discovering new cathode materials. The number of possible compositions increases combinatorially with the increasing number of elements, and the computational and time cost for an exhaustive exploration quickly becomes prohibitively high.[143] It is often necessary to limit the search space based on expected oxidation states, theoretical cycle capacity and cost of the raw materials. Constructing pseudobinary/pseudoternary systems can be a viable option to mitigate the *curse of dimensionality*. Choosing the right system to explore is crucial, and selecting such systems remains reliant on the domain knowledge of the researchers.

Obtaining the crystal structure is just the first step towards a comprehensive understanding of a material. There is also a lack of accurate descriptors for cathode performance purely based on atomistic models. For example, the real energy density of a cathode depends on the number of Li that can *reversibly be removed* (per f.u.) and its corresponding voltage. Such a value is relevant not only to the oxidation states of the TM ions, but also to the structural stability after the Li atoms have been removed, which is difficult to capture efficiently using atomistic models. Beyond that, the rate capability of the cathode relies on several factors beyond the Li energy barrier such as the percolative property of Li diffusion paths, which is not easy to quantify accurately.

Recent progress in a range of materials research communities can be utilised to help meet the challenge of predicting novel cathode materials. For instance, the development of better exchange-correlation functionals improves the accuracy of DFT calculations.[144,145] While density functional theory is still the go-to method for atomic-level predictive modelling, it suffers from its inherent cubic scaling nature. Methods of constructing interatomic potentials or forcefields using machine learning have been developed to tackle this problem.[146,147] Using first-principles calculations as the training data, these forcefields are capable of achieving the same level of accuracy with orders of magnitude lower computational costs. Pioneering works have demonstrated that the resulting potentials can be used for predicting new crystal structures.[148] Building such potentials from scratch, however, is still not a trivial process, so developing robust and automated fitting workflows could help access these state-of-the-art techniques. The local environment descriptors, originally introduced for these potentials, turned out to be invaluable tools for analysing a large number of structures routinely generated during structure prediction.[149]

The development of efficient and standardised searching protocols will help improve search efficiency. Since intercalation type cathode materials are predominately ionic, a significant part of the total energy comes from the long-range Coulomb interactions. While classical interatomic potentials may not be transferable enough for predicting entirely new phases, they do capture a significant portion of the underlying interactions. It may be possible to use them for removing structures that are not “sensible” and deemed to end up with high energies.

The success of structure prediction undoubtedly relies on the identification of the promising chemical space to explore in the first space. Existing computational material databases such as the Materials Project[150] and the Open Quantum Material Database[151] are useful tools for researchers to quickly identify the explored and underexplored regions, acting as *entry points* for new studies, and providing data to build property-driven machine learning models.[152] The development of simple and physical descriptors, such as site-specific electrostatic energies[153] and specific “structure units”,[154] would also help to tease out the underlying structure-property relationships to provide a fundamental understanding of existing and new cathode systems.

Concluding remarks

The development in structure prediction and first-principles methods has made it possible to discover new materials before they even come into existence. While there are challenges ahead for applying it to cathode materials, the development of new methodologies and technologies from the wider research community will continue to benefit this field. In the near term, the computational cost will remain the bottleneck for scaling up its application in complex materials systems. Search algorithms that are inherently parallel, such as AIRSS, will receive the full benefit of the upcoming transition to "exascale" multi-core massively parallel computing platforms. Identifying promising chemical systems is also crucial for searching to succeed. Crystal structure prediction offers a unique opportunity to dramatically enhance the breadth and rate of materials discovery, providing novel compositions and fundamental understanding to both complement and direct experimental work.

7. Enhancing Lifetime through Gradient and Core-Shell Structures

Nirmalesh N. Anthonisamy, Rebecca Boston and Serena A. Corr

As previously discussed, there exist numerous cathode materials that display high capacities, but for which remaining challenges exist around structural degradation, thermal instability and/or reaction with the electrolyte. These processes can lead to capacity fade, often including oxygen evolution at the cathode/electrolyte interface, which has implications for the longevity and safety of the battery. As a first line of defense, surface coatings may be employed to curtail these processes. Such coatings can be applied through simple sol-gel or hydrothermal methods, although it can be challenging to provide conformal coatings via these methods. By comparison, superior ultrathin nano-level coatings can be obtained using state-of-the-art chemical vapor deposition (CVD) and atomic layer deposition (ALD) techniques.[155] Scalability then becomes a challenge to overcome. In light of this, core-shell and concentration-gradient structures have emerged as an efficient alternative in tackling degradation issues.

Choice of synthetic pathway can facilitate the introduction of a core-shell or concentration-gradient arrangement to cathode particles. Co-precipitation of a multi-component Ni-rich materials (e.g., NMC811) from solution via a continuous stirred tank reaction (CSTR), for example, affords an approach that combines the necessity of atomic-level mixing of constituent elements with the potential to generate core-shell and concentration-gradient structures due to its potential to fabricate unique highly dense, spherical precursors. Importantly, a CSTR permits large-scale production of cathode materials facilitating material advancement from lab to industry. Hydroxide, carbonate or oxalate metal precursors can be used, with hydroxides playing a particularly important role in achieving core-shell and concentration-gradient materials. In the case of hydroxides, the solubility product constant (K_{SP}) of $Mn(OH)_2$ is two orders higher than that of $Ni(OH)_2$ and $Co(OH)_2$.[156] Therefore, ammonia is used as a complexing agent to achieve the required atomic distribution of nickel, manganese and cobalt ions. The pioneering works of Dahn and Sun [157,158] have established the growth mechanism of secondary spherical particles in the presence of ammonia as follows (i) the reaction begins with the metal-ammonia complex formation (ii) of which the ammonia ions are gradually replaced by hydroxide ions via anion-exchange reaction (iii) then due to coalescence and Ostwald-ripening the primary nanocrystals self-assemble into micron-sized spherical hydroxide precursor. The surface free energy reduction is the key driving force that benefits the growth of larger particles at the cost of smaller particles through dissolution and recrystallization.

Core-shell materials are typically designed in such a way that a high-capacity (Ni-rich or Li-rich), less stable material is at the core, with a thermally stable (Mn-rich) material as the shell. The main requirements for a successful core-shell structure are high density, low layer inter-diffusion, good inter-layer adhesion, and compatible rates of expansion/contraction during (de)intercalation. High density of both the core and shell is critical to ensure mechanical stability along with high energy density, as any voids equate to lost active material.[159] The core-shell materials can be broadly classified into two types (i) pairs with similar crystal structure and chemical composition (layer-layer, spinel-spinel, olivine-olivine etc.) and (ii) either dissimilar crystal structure or chemical species (layer-spinel, layer-olivine, oxides-phosphates etc.). An ideal shell material should be versatile enough to overcome those shortcomings of the core including: lattice-oxygen evolution, transition metal dissolution at the surface promoting secondary phase formation, and impedance growth at the interface in a fully de-lithiated state. Therefore, the choice of shell material largely depends on the type of challenges one wishes to address with the core material.

For example, in 2005, Sun *et al* demonstrated that the thermal stability of Ni-rich high capacity NMC811 can be substantially improved by coupling it with a Mn-rich $\mathrm{LiNi_{0.5}Mn_{0.5}O_2}$ shell. The core-shell material exhibited reduced heat generation of 2261 J/g at 250 °C at a charged state to 4.3 V in contrast to 3285 J/g at 180 °C found for the pristine material.[159] Consequently, the cycling stability of the core-shell material was considerably higher than the pristine materials (98% vs. 81%) after 500 cycles. In another work, Yuan *et al* have shown that at high voltages (4.5 V) it is possible to alleviate the layered to rock-salt like phase transformation in $\mathrm{LiNi_{0.5}Mn_{0.3}Co_{0.2}O_2}$ (NMC532) by shielding this with a layer of NASICON type-$\mathrm{NaTi_2(PO_4)_3}$ shell material.[160] This shell has proven effective against HF attack, which would give rise to the dissolution of electroactive elements from the surface regions. With 5% Mn-rich $\mathrm{Li_{0.65}Mn_{0.59}Ni_{0.12}Co_{0.13}O_\delta}$ (LMNCO) on NMC811, a nearly one order of magnitude decrease of interfacial charge transfer resistance was reported by Zhao *et al.*[161] As a result, the core shell material delivered a remarkable capacity of 150 mAh/g at 5C rate (1C=200 mA/g) with 83.4% retention after 500 cycles. A novel double shelled material $(\mathrm{Li}\{[(\mathrm{Ni_{0.8}Co_{0.1}Mn_{0.1}})_{2/7}]_{\mathrm{core}}[(\mathrm{Ni_{1/3}Co_{1/3}Mn_{1/3}})_{3/14}]_{\mathrm{shell1}}[(\mathrm{Ni_{0.4}Co_{0.2}Mn_{0.4}})_{1/2}]_{\mathrm{shell2}}\}\mathrm{O_2})$ was tailored by Zhang *et al* in which one of the shells ($[(\mathrm{Ni_{1/3}Co_{1/3}Mn_{1/3}})_{3/14}]_{\mathrm{shell1}}$) improves the rate capability and the other ($[(\mathrm{Ni_{0.4}Co_{0.2}Mn_{0.4}})_{1/2}]_{\mathrm{shell2}}$) contributes to the cycling stability of the hybrid structure. The double shelled material displayed superior electrochemical performance in comparison to the homogenous compound with the same average composition ($\mathrm{Li(Ni_{0.5}Co_{0.2}Mn_{0.3})O_2}$).[162]

Structural or chemical mismatch between the core and the shell could lead to voids between the two components, hindering $\mathrm{Li^+}$ ion diffusivity and electron transport. Additionally, such voids may generate chemical pressures leading to compositional variations that can form a blocking layer, shielding the core entirely. Concentration-gradient materials may be applied to try to overcome these challenges, where the transition metal cation concentration varies radially from an area of higher to lower concentration. In the case of nickel-rich cathodes exhibiting concentration-gradients, one can experimentally visualize a Ni-rich solution 1 is pumped into the reactor to form the core, after which a more Ni-poor solution 2 is pumped into solution 1 and simultaneously the mixture is injected into the reactor to give rise to a concentration-gradient. This strategy was demonstrated by Sun *et al* in 2009 by synthesizing $LiNi_{0.8}Mn_{0.1}Co_{0.1}O_2$ core and $LiNi_{0.46}Co_{0.23}Mn_{0.31}O_2$ surface composition by pumping 0.08:0.46:0.46 of Ni-Mn-Co molar solutions (solution 2) into 0.8:0.1:0.1 molar solution (solution 1) resulting in a constant core and concentration-gradient shell. This concentration-gradient cathode material delivered a high specific capacity of 200 mAh/g in contrast to 142 mAh/g exhibited by the pristine material after 50 cycles within a 3.0-4.4 V voltage range at 55 ^{o}C.[163] Interestingly, the authors reported a shrinking in the core and an expansion in the shell during the subsequent high temperature calcination process, which may be attributed to the inter-diffusion of the transition metal cations. To resolve this and further boost the electrochemical traits of concentration-gradient materials, a new full concentration gradient (FCG) material was proposed where the Ni and Mn concentration varies continuously resulting in a Ni-rich core and Mn-rich shell and an average composition $LiNi_{0.75}Mn_{0.15}Co_{0.10}O_2$. Owing to the FCG nature and needle-like nanostructure, the material exhibited a high specific capacity of 215 mAh/g and excellent capacity retention of 90% after 1000 cycles.[164] In 2015, Sun et al further extended this concept by introducing two slopes of transition metal ion concentration within the particle (termed TSFCG). The synthesis of these TSFCG is achieved by sequential addition of two Mn-rich solutions (solution 2 molar ratio 0.68:0.11:0.21 and solution 3 molar ratio 0.51:0.20:0.29 of Ni-Co-Mn) at regular intervals to the Ni-rich core solution (solution 1 molar ratio 0.8:0.05:0.15 of Ni-Co-Mn). The materials obtained by this approach delivered a high specific capacity of 200 mAh/g and superior cycling stability of 88% for 1500 cycles in a full-cell configuration.[165] Efforts to simplify the process of introducing concentration-gradients include work by Zhang *et al* who proposed an alternative approach by first preparing a double-shelled precursor material followed by tuning of the subsequent calcination temperature or duration to promote the inter-diffusion of transition metal cations, yielding an internal concentration gradient.[166]

Concluding remarks

A recent study on pinpointing the major degradation mechanism governing the capacity loss in NMC811 has discussed in detail the formation of fatigue phase in aged electrodes. The active-bulk lattice planes of layered structure pinned to the surface-reconstructed rock-salt like NiO that constrain lattice dynamics during Li^+ extraction is responsible for the generation of this fatigue phase, particularly at high states of charge (SOC >75%).[167] These findings further emphasize the significance of developing novel core-shell or concentration-gradient structures to mitigate these processes. Although they can be challenging to produce, core-shell and concentration-gradient structures offer a route to the use of high capacity, but oft-times unstable, compositions. As the Li-content of NMC is pushed higher, there is a general trend to lower stability, and so core-shell or concentration-gradient structures may represent a means to exploit these high Li compositions whilst minimizing decomposition. Similarly, new compositions may not be immediately compatible with existing electrolytes, and so the means to provide a passivating but still electrochemically active surfaces may become increasingly important. Using first principle calculations, Yao *et al* have also shown that by appropriate choice of core and shell material one could exploit the high Li diffusivity originating from difference in Gibbs free energy, which opens up an enticing new avenue of material design for fast-charging requirements.[168]

8. Advances in Performance through Hierarchical Structuring of Electrodes

Seungkyu Park and Michael De Volder

As set out in earlier sections, cathodes materials are achieving ever higher operating voltages and gravimetric energy densities. However, to be commercially viable, several additional factors need to be considered, including how these materials are formulated and manufactured in a practical electrode. First, transition metal oxide cathodes tend to have intrinsically low electronic conductivities ($10^{-10} \sim 10^{-8}$ S/m),[169] which can cause non-uniform charge distributions in the electrode. To alleviate potential inhomogeneous states of charge, optimization of electrode composition and material design such as coating with conductive polymers or carbonaceous substances, as well as methods to incorporate advanced conductive additives to the electrodes have been intensively researched.[170-175] Furthermore, certain newly developed cathode materials consist of particles with low packing densities, resulting in reduced overall volumetric energy densities, despite advances in the gravimetric energy density.

For many electrode materials, a popular strategy for enhancing electrical conductivity is coating the surface with a conductive carbon layer. However, for a number of materials, this process is not well suited. This is because the pyrolysis reactions generally used to create carbon coatings tend to scavenge oxygen from the cathode material, forming CO_2.[170] These reactions typically degrade the cathode performance. To address this challenge, there is a substantial amount of work invested in the development of carbon coating methods for advanced cathodes at relatively low temperature (< 600°C).[173,176] Another key challenge involves coating uniformity. Many cathodes consist of secondary aggregates of nano-sized primary particles and most carbon coating methods will only coat the outer surface of the secondary particles. As a result, electron transport to primary particles located in the center of secondary particles often remains problematic.[177]

Both the conductive additives and binders required for most cathodes to perform effectively do not take part in the charge storage process, so excessive use of these materials leads to a decrease in the overall energy density of the cell. In addition, the large surface area of certain additives can lead to side reactions with the electrolyte. Conversely, too little conductive additive or binder can lead to insufficient electric conductivity and poor mechanical integrity. This contributes to a complex optimization process, which not only affects the volumetric capacity, but also has a significant impact on rate performance and cycling stability. The latter is illustrated in **Figure 8**, which shows an example of capacity fade for a spinel structured $LiMn_2O_4$ cathode with cycling (**Figure 8a**) and EIS spectra (**Figure 8b**) when varying the binder and conductive additive compositions.[178]

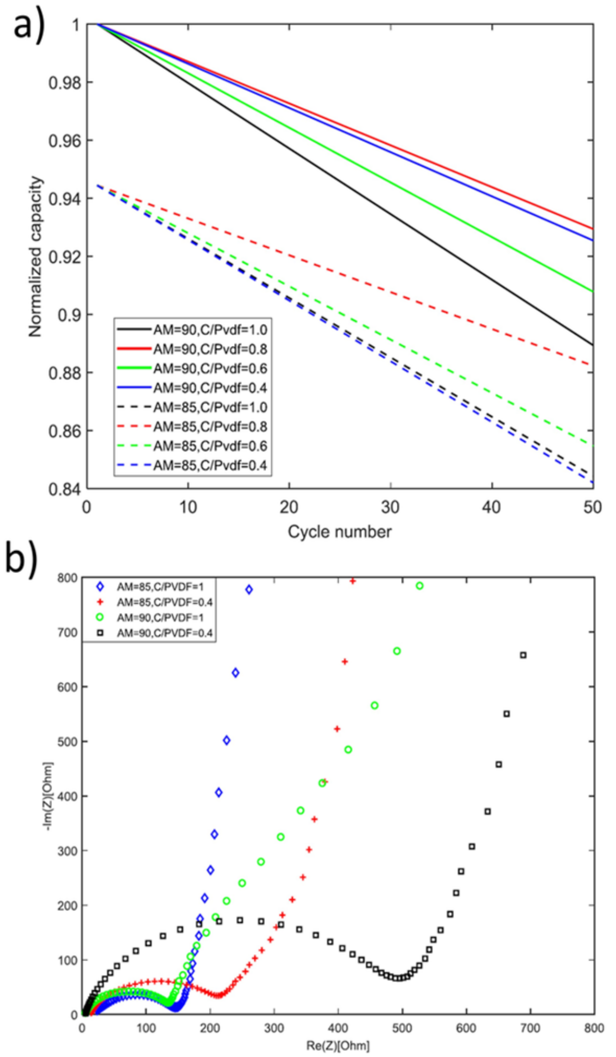

Figure 8. a) Normalized capacity as a function of cycling for $LiMn_2O_4$ and b) EIS spectra with different electrode composition. The electrode composition presents that active material (AM) e.g. 90% for AM=90 and the ratio of conductive material and binder for C/PVDF. Reproduced with permission from MDPI, Basel, Switzerland.

In an idealised model, every individual particle has the same state of charge (SOC) at any given time during the cell operation. However, these conditions are rarely met due to the presence of inhomogeneity in the conductive network as discussed above, as well as heterogeneity in the particle size distribution, electrolyte exposure, phase transitions, and electrolyte decomposition products.[179,180] The variations in lithium-ion access and electrical contact result in macroscale SOC inhomogeneities across the entire electrode during cycling. For example, the primary particles located in the center of secondary particles have comparatively large electric resistance, lacking direct contact with the conductive additives. Furthermore, the chemical environment of the primary particles varies from secondary particle core to surface, leading to further nanoscale SOC inhomogeneity. These different sources of SOC variability are problematic as they are difficult to control and quantify, whilst significantly impinging on the electrode performance and contributing to degradation.

Substantial academic and industrial effort is being exerted towards addressing the challenges described. For instance, recently reported oxidative chemical vapor deposition (oCVD) techniques using 3,4-ethylenedioxythiophene (EDOT) monomers and vanadium oxytrichloride ($VOCl_3$) oxidant vapors at 90°C have shown the ability to coat ultraconformal conductive poly(3,4-ethylenedioxythiophene) (PEDOT) skins on the surface of primary or secondary particles.[181] Material structuring techniques such as spray drying are also being developed for cathode films to improve the packing density of nanoparticles.[182,183] A particular challenge with some of the more advanced material organisation techniques is that they are not compatible with conventional electrode mixing and coating methods. In a limited number of examples advanced material structuring has been demonstrated through techniques such as continuous roll-to-roll coating.[184] Looking forward, key developments will rely on new hierarchical electrode designs that revisit how we pack materials more densely in electrodes without compromising the electron and ion transport.

Concluding remarks

The development of new cathode materials, with a focus only on the electrochemical performance of thin electrode coatings comprising large amounts of conductive additive risks significant issues in later development when testing against industrial requirements. The high areal loadings, high volumetric densities and low quantities of conductive additive and binder required, serve to increases the performance threshold for suitable cathode materials. For example, a novel cathode material which is unable to form a dense packing structure may see a reduced volumetric capacity even if the specific performance of the material is improved. The same is true for materials that require excessive amounts of conductive additive or binder to operate reliably. Therefore, managing the electronic and ionic transport through the electrode needs to be judiciously controlled. This is an area where, for instance, finite element simulations of the electrodes can play an important role. Finally, these efforts need to be orchestrated with optimisation of the material morphology. In the case of nanosized materials, issues in volumetric performance and possible side reactions with the electrolyte necessitate techniques to pack these materials into secondary structures, allowing for efficient coating with high areal loading and packing density. Ultimately though, micrometer sized, single crystal cathode particles offer even higher volumetric densities and these are therefore playing a key role in the further development of advanced cathodes. The significance of single crystal particle morphologies in further underlined in the mechanical strength section below. By optimising synthetic approaches to fabricate large single crystals materials, and efficient techniques to assemble dense secondary structures, we can push the performance and lifetime of these materials, along with minimising the reliance on non-active electrode components.[32]

9. Understanding the Role of Interfaces

Venkat Daramalla, Debasis Nayak, Abby R. Haworth, Hugo Bronstein, John M. Griffin, Judith MacManus-Driscoll and Siân Dutton

As discussed in the previous sections, achieving a high energy density and high operating voltage is key to cathode development, aiming for real terms improvements in \$/kWh. Performance improvements within the material often come at the cost of reduced stability and an increase in detrimental side reactions. Investigations into high nickel content in the layered cathodes and through spinel materials show that it is particularly important to mitigate the challenges these classes of materials suffer during cycling, to achieve high performance. Significantly, the surface of nickel-rich compositions is very sensitive to the atmosphere and an increase in charge-transfer resistance is often observed during cycling. This is particularly due to structural instability and formation of non-electroacive species through side reactions that occur at the electrode-electrolyte interface. In addition, metal dissolution at a high operating voltage (>4.7 V), capacity fade at elevated temperature, and Li^+-consumption at the SEI in high spinel cathodes are other problems that need to be addressed.[185] Li extraction/insertion in Ni rich cathode materials also causes a strong anisotropy in crystal structure leading to chemo-mechanical degradation and bulk fatigue at the surface.[167]. Spinel-type materials also suffer from bulk and surface instabilities at high charge states, issues common to the majority of cathode materials.

The interface between the electrode and electrolyte is one of the vital components of the battery and must remain stable enough for safe operation and to avoid performance degradation. A functioning CEI structure provides an unimpeded passage for Li^+ charge transfer from the electrode to the electrolyte. The electrode/electrolyte interaction can suffer from parasitic reactions in the case of liquid electrolytes and the formation of a space charge layer in the case of solid electrolytes.[186,187] Surface coatings (or also known as surface stabilisation or surface coating/modification in the wider scientific literature) are a promising solution to address these challenges. An interface layer or coating acts as a bridge or “pseudo electrolyte” between the electrode and electrolyte and protects from any unwanted reactions in the battery cell.[188] Cathode coatings offer a number of beneficial target properties that include: improvements to the structure, morphological stability, Li-ion transport, and thus electrochemical performance (cycling performance and rate performance at high current densities) of battery electrodes. The coating can prevent unwanted side reactions and act as a scavenger for any HF, reducing the acidity of non-aqueous electrolytes. Similarly, the coating can mitigate/protect or suppress the metal dissolution (TM/Li-migration) from the cathode. Such improvements can allow for higher performance and operation with an increased cut-off voltage.

There are numerous inorganic materials explored and experimentally tested as interfacial coatings on different classes of cathode materials in the scientific literature. These include (i) single element interfaces such as carbon,[189] and titanium,[190] (ii) binary oxides ZrO_2,[191] ZnO,[192] TiO_2 [193]and Al_2O_3,[194] (iii) composite oxides,[195] and (iv) even some battery electrodes,[196] and electrolytes ($Li_4Ti_5O_{12}$, $LiNbO_3$, Li_3PO_4, & LiPON).[197,198] Each of these materials offers different functionalities and challenges depending on the particular cathode chemistry, other battery-cell components, and coating method. This is a very active area, with several review articles and perspectives available in the literature, along with many research articles.[198-202] Herein, we lay out the experimental design principles to form an effective artificial CEI. This is important when looking to screen or select the correct materials for an ideal coating:

i) An ideal interfacial layer should be electrochemically and chemically inactive whilst providing adequate Li-ion transport across the interface - offering a homogeneous microstructure with good mechanical & thermal stability. A homogeneous microstructure coating is required to facilitate uniform Li-ion diffusion (or electron-conduction media) across the electrode-electrolyte, and offers complete coverage of the cathode particles.

ii) Provide sufficient adhesion between liquid (solid)-electrolyte and cathode/anode electrodes, and should not participate in any direct reaction with lithium (Li-ion intercalation/deintercalation during the battery operation).

iii) Provide low-interfacial resistance, long-term stability, and safety during the operation of batteries at standard operating and elevated temperatures.

iv) Compatibility with the specific industrial scaling process depending on the battery chemistry, and manufacturing process, coating technology, and thermal budget (i.e. compatible with processing conditions of the cathode, electrolyte, anode, current collectors and final battery packaging).

v) Must not directly or indirectly participate in any adverse chemical reactions with both cathode and electrolyte components (salts, solvents, and additives).

vi) Ideally, the interface should be formed during the battery operation (for example, similar to SEI formation). The CEI should act as a passivation layer allowing adequate Li-ion transport across the interface at operating voltage of the battery.

vii) Finally, it should help contribute to rather than detract from the performance indicators required of next generation cathode materials (such as offering good ion-transport, high capacity, structural and morphological stability at high current densities, long cycle life, safe operation, cost-effectiveness and recyclability and should have minimal or zero adverse effects on the operation of the Li-ion battery in the long-term (operation or storage).

An appropriate film that can satisfy all ideal requirements stated above is yet to be achieved. What is clear is that the artificial CEI can alleviate some of the performance issues raised previously, however, this usually comes at the expense of a different property or significant increases in the non-active mass within the cell. A promising recent coating example, $LiAlF_4$ has been examined as a coating on NMC811.[188] However, the performance of NMC811 could yet offer further improvements by reducing the effect of bulk fatigue at the surface. Alongside the stability of the cathode, coatings that enable high voltages in liquid electrolyte cells will benefit layered materials, spinels, disordered rocksalts and numerous new cathode chemistries.

When examining possible artificial CEI materials, numerous suitable materials must often be screened. The interfacial layers must be tuned to the specific behavior of the cathode material (nickel rich layered materials, disordered rocksalts, spinels, and multi-anion cathode materials). The structure, morphology and thickness of the coating must be optimised. With key considerations of the underlying cathode particle size and morphology. Aiming to enables high ion conduction, high capacity, thermal stability, a stable structure, and high cut-off voltage at high current rates.

To understand and develop suitable cathode coatings, a fundamental understanding of the interactions that occur at the buried cathode/CEI interface is required. This can be approached in two distinct manners – through computational simulations of the interfaces, or through the synthetic development of ideal cathode interfaces for advanced characterisation. An AIRSS approach, as described previously, can provide structural models along with in depth DFT calculations, however, for such studies, a sound synthetic model is initially required as such complex interfacial interactions may stray from the thermodynamic minima.

Ideal cathode interfaces for such investigations can be produced through formation of epitaxial or highly calligraphically oriented cathode thin film electrodes. Enabling the study of anisotropic distortions or structural transitions (nickel rich layered materials), isotropic volume changes (disordered rocksalts), or diffusion properties through specific crystallographic planes (spinels). Such thin film cathode materials offer an ideal substrate to study coating interactions, detailed ion transport behavior, structure and electrochemical properties. A combined understanding of such films both computationally and experimentally will help to advance progress towards optimization of cathode coatings.

Using DNP NMR Spectroscopy to Probe Surfaces and Interfaces in Batteries and Battery Materials

Fully understanding structures and processes at interfaces is crucial to the advancement of battery research. However, these can be challenging to probe as they make up a small proportion of the sample and are often complex and disordered in nature. As solid-state NMR spectroscopy is a versatile, non-destructive technique with no requirement for long-range order, it has the potential to provide valuable insight into such interfaces. Unfortunately, intrinsic sensitivity limits can prove challenging to overcome. Recently, dynamic nuclear polarisation (DNP) has emerged as a powerful technique for sensitivity enhancement in NMR experiments. In DNP, polarisation is transferred from an unpaired electron to surrounding nuclear spins at cryogenic temperatures. This technique is extremely promising for studying surfaces and interfaces which, without enhancement, may be impossible to observe using conventional NMR spectroscopy. Hence, it has recently gained interest in a number of research areas.[203-205]

Typically, unpaired electrons are introduced to the system via a solution of organic radicals, *e.g.*, TOTAPOL,[206] which is added to the powdered solid sample. As the radical is external to the sample of interest, the polarisation spreads from the surface of the particles into the bulk. As a result, DNP experiments can provide surface-selective enhancement. For example, the first three surface layers of CeO_2 nanoparticles can be probed using ^{17}O MAS-DNP NMR experiments.[207] Additionally, DNP experiments have been used to study the solid electrolyte interphase (SEI) layer that forms on reduced graphene oxide and silicon anodes.[208,209] However, despite its promise, DNP has its limitations. Most notably, the addition of the radial solution may alter the system, which may be problematic for reactive or unstable samples such as battery electrodes. Recently, alternative approaches have been developed such as introducing paramagnetic ions as dopants into the bulk of the sample, allowing polarisation to be transferred directly to neighbouring nuclei. Using this approach, ^{17}O MAS-DNP NMR data has been acquired for anode materials, including $Li_4Ti_5O_{12}$ and $Li_2ZnTi_3O_8$, without costly isotopic enrichment.[210,211] Recently, DNP has allowed observation of the interface between the SEI that is deposited onto lithium metal anodes during cycling. The selective enhancement of this interface was achieved by utilising the metallic electrons with the lithium metal as the polarisation source.[212] The increased sensitivity afforded by DNP is extremely encouraging and provides an exciting opportunity to probe cathode-related interfaces, which in turn is promising for the advancement of battery research.

Concluding remarks

In order to understand the material's intrinsic characteristics and resolve the associated challenges, it is essential to study the electrochemical behavior of binder and additive-free electrodes. Again, to understand the role of the interface between the electrode and electrolyte and modify the surface strategically, thin-film fabrication of the electrodes is the way out. The interface study and engineered modification of surfaces can enable measurement of the fundamental properties of the system in isolation, and offer improved cycling performance. In this regard, advanced techniques such as DNP NMR spectroscopy can be used to understand the interface and the effect of different coating materials in enabling enhanced cycle stability and safer operation of the electrode material.

10. Advances in *Operando* Characterisation of Cathodes

i. Structural Analysis

Gabriel E. Pérez, Helen Y. Playford and Stephen Hull

Investigation of the structural changes that the cathode experiences during battery operation is paramount to understand their role in the performance and stability of the device, and consequently, to improve the cathode design to develop more capable and lasting batteries. Due to their arguably unmatched ability to provide atomic-scale information with high detail and accuracy, diffraction techniques have been the go-to methodologies to study the structure of cathodes. Specifically, X-ray and neutron diffraction have been effectively used as complementary techniques to study complex cathode structures due to the distinct physical interactions between each probe and the motifs within the unit cell of a given crystal structure. While X-rays interact almost exclusively with the electron cloud of atoms, neutrons can interact with the atom's nucleus to provide structural information, or the atom's electron cloud to provide information on the magnetic properties of the sample.

In the simplest type of diffraction experiment, the cathode sample of interest is investigated before and after applying some environmental and/or operational conditions to it. A slightly more sophisticated variation of this study involves the use of *in situ* temperature and pressure modifiers such as furnaces, cryostats, or diamond anvils that are compatible with the experimental setup, allowing the collection of the diffraction pattern while such conditions are applied. However, these experiments are unable to provide crucial information about the structural changes that the cathode experiences during battery operation. For such information, one must look to electrochemical control through *in situ* or *operando* type diffraction experiments. Whereby, both the environmental and operational conditions that the cathode experiences in its intended real application are reproduced as closely as possible, while the structure is examined. This requires the design and fabrication of *in situ*/*operando* cells which closely replicate the electrochemical stimulus provided in a standard battery cell, while ensuring meaningful diffraction data from the cathode. This can pose an engineering challenge when it comes to required modifications of the cathode geometry or composition, materials requirements for the inspection windows and stability under vacuum. These conditions must be tempered against those of a suitable electrochemical cell; in the case of cathode materials, which are often poor electronic conductors, the window should ideally function as the current collector to ensure that the reaction of interest is occurring at the point of inspection.[213] Despite the strict requirements of the cell, *in situ*/*operando* diffraction experiments provide a unique route towards mechanistic understanding of processes occurring at high states of charge or on repeat cycling. Therefore, there is a significant interest in the further optimisation of existing cell designs, along with the development of novel cells to enable access to additional unexplored techniques or refined combinatorial measurements - for instance scattering in conjunction with spectroscopy.

Evidently, obtaining a high-intensity and high-resolution diffraction pattern is crucial for the correct analysis of the cathode structure. In the first instance, this requires the collection of a significant number of probe-cathode interactions. For X-ray experiments, bench top experiments using soft X-ray sources have been around for a significant amount of time, and there exist several suitable *in situ* cell designs. Synchrotron sources by comparison offer significant enhancements in flux and therefore detection time, resolution and more flexible cell design due to the higher penetration depth of the X-rays. Tunable X-ray energies allow for resonant diffraction measurements, and the development of specialist detectors also enhance the possible Q space range that can be gathered which is hugely significant for total scattering analysis. However, beam damage to the cell's materials must be considered due to the highly energetic X-rays.

Neutrons are naturally highly penetrating, however the typical incident flux at a neutron source is significantly lower than that of X-ray sources, especially synchrotron sources. This increases the duration of the experiment and often requires the use of large samples, in the range of cm^3. For cathode materials, this can offer a significant challenge. In addition to this, to fully exploit the advantageous isotopically dependent scattering of neutrons, labelling techniques such as deuteration are often required, especially when determining the location of some atoms within the cathode. Deuteration is also needed to reduce the level of incoherent neutron scattering from highly hydrogenous materials in the cell. Regardless of the purpose for deuteration, the synthesis of deuterated materials can be complex and expensive.

In addition to the previous considerations, cells need to be easily assembled/disassembled, highly reproducible for further electrochemical testing, and adaptable to the specific instrumentation in which they will be used. As synchrotron facilities continue to invest in upgrades, the significance of limitations in measurement time diminish, with more and more techniques reaching time resolutions which can examine fast charge/discharge processes to understand the implications of higher power operation on battery cathode materials.

The most effective approach to address the challenges previously described has been to focus on the design of an *in situ/operando* cell. Cells for X-ray diffraction can be designed for either soft or hard X-rays, and for reflection or transmission mode (**Figure 9**). One of the most popular designs, due to its widespread applicability, is the 'coin cell' whose designated probing area has one (for reflection mode) or two (for transmission mode) X-ray-transparent windows.[214] Coin cells owe their popularity to their low cost, simple assembly and good sealing: therefore, there are many variations of this type of cell. For instance, for the detection window, beryllium is highly toxic and is often replaced with a different material such as a Kapton film (polyamide)[215] which is highly transparent to X-rays and chemically inert. As a non-conductive material, the applicability of the response in this region of the cathode must be considered carefully. This can be mitigated by reducing the window size, adding a conductive mesh, or increasing the amount of conductive additive in the cathode. For large inspection windows, measurements in different regions within the window, or ex situ measurements of the cathode afterwards are good practice to ensure uniformity of response. The AMPIX cell, developed by researchers at the Advanced Photon Source in the US, uses a glassy carbon inspection window to ensure uniform electrochemistry through the cathode.[213] More specialist cell designs have been developed to mimic cylindrical cell designs such as the 18650 cell,[216] and the cylindrical RATIX cell.[217] When larger cathode areas are required, or to minimise unwanted scattering form non-cathode materials, a pouch or "coffee bag" cell design is often employed. To avoid cell damage from the highly energetic hard X-rays, intermittent sampling or different region probing is often utilised as good practice.

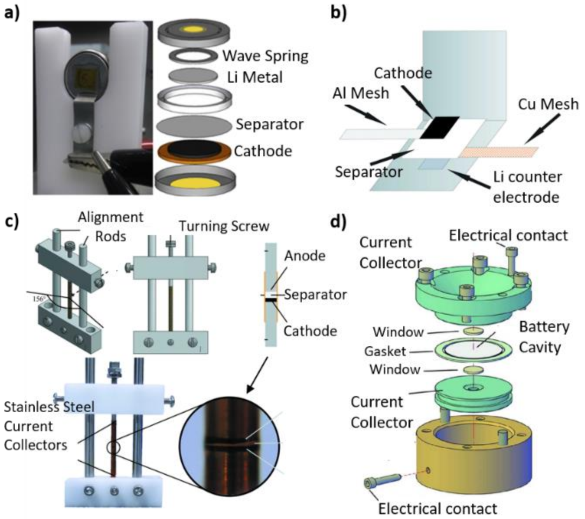

Figure 9. a) A coin cell, along with its schematic representation, mounted on a specially designed holder for the powder diffraction beamline at the Australian Synchrotron. (Reprinted from J. Power Sources, Vol 302, Brant, Li, Gu, and Schmid, Comparative analysis of ex-situ and operando X-ray diffraction experiments for lithium insertion materials, 126-134., Copyright (2016), with permission from Elsevier.) b) Schematic representation of a coffee bag cell before sealing. c) Schematic representation of the cylindrical RATIX cell. d) Schematic representation of the AMPIX cell. Reproduced with permission of the International Union of Crystallography from Refs. 218 [Rosciano, Holzapfel, Kaiser, Scheifele, Ruch, Hahn, Kötz, and Novák, Journal of Synchrotron Radiation (2007)], 217 [Liu, Allan, Borkiewicz, Kurtz, Grey, Chapman, and Chupas, Journal of Applied Crystallography (2016)] and 213 [Borkiewicz, Shyam, Wiaderek, Kurtz, Chupas, and Chapman, Journal of Applied Crystallography (2012)] respectively under the Creative Commons Attribution CC BY 4.0.

Most of the previously mentioned type of cells are also been used for neutron diffraction experiments; however, the design of a specific cell has been driven by additional factors. In neutron experiments, to minimise incoherent scattering, it is common to use deuterated electrolytes and fluorinated separators.[219] The wider range of neutron transparent materials mean that it is often easier to maintain good electrochemical performance, utilising inspection windows that act as the current collector, for instance Ti-Zr alloy or Al.[220] Additionally, time-of-flight diffractometers available at pulsed neutron sources such as ISIS Neutron and Muon Source in the UK allow the collection of the diffraction pattern at fixed scattering angles. This fixed geometry makes it possible to define a scattering volume strictly within the sample by collimating the incident and scattered beam, and thus, eliminate Bragg peaks from surrounding components (**Figure 10**). The key drawback for *in situ* neutron experiments, as touched on before, is the very high sample mass requirements. This can be hard to achieve in a planar cathode electrode, and thus there is significant room for further optimisation in this area.

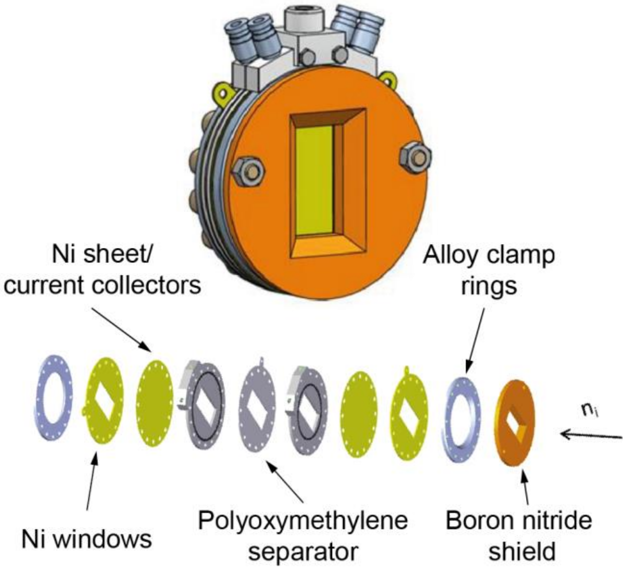

Figure 10. Diagram of an in situ cell used in the POLARIS diffractometer at the ISIS neutron spallation source. Reprinted from Journal of Power Sources, Vol 248, Biendicho, Roberts, Offer, Noréus, Widenkvist, Smith, Svensson, Edström, Norberg, Eriksson, and Hull, New in-situ neutron diffraction cell for electrode materials, 900-904., Copyright (2014), with permission from Elsevier.

Concluding remarks

In situ/operando diffraction techniques can provide detailed and accurate information about the crystal structure of the cathode during battery operation providing the experiment, especially the cell, is carefully designed to obtain reliable information. However, even when the ideal experimental conditions for an *in situ/operando* diffraction experiment are met, many candidate next generation cathode materials offer complex structures which are not possible to resolve through conventional diffraction alone. This is due to the disordered nature of the crystal structure of some cathodes, with the likely presence of cation and anion disorder increasing with the complexity of the cathode chemistry and processing conditions. In such cases, other experimental techniques such as neutron/X-ray imaging, and data analysis techniques such as atomic pair distribution function (PDF), should be considered. Regardless of the chosen technique, the same considerations for the *in situ/operando* experimental design should be taken for high quality data collection.

ii. Understanding the Role of Disorder

Harry S. Geddes and Andrew L. Goodwin

The structural and compositional complexity of cathode materials present clear challenges for characterisation. Many of these difficulties are exacerbated in the presence of disorder — not least because classical crystallographic approaches are inadequate in such cases. Instead, local structure probes such as NMR and total scattering are increasingly relied upon in order to provide accurate structural descriptions of cathode materials. Moreover, a complete understanding of cathode function means characterising the dynamic processes involved in cycling: the complex phase evolution that occurs during lithium insertion and removal.

In situ and *operando* measurements are designed to replicate as closely as possible the native operating environment in a working battery. Doing so helps identify and track the key phase transformations that occur during battery cycling — including the presence and role of transient phases otherwise hidden from *ex situ* characterisation. An excellent example of the state-of-the-art in this respect is the discovery of transient Li_xFePO_4 ($0 < x < 1$) solid solutions that are present during rapid cycling of the commercially-important $LiFePO_4$-Li battery. These transient phases subsequently relax to a mixture of stoichiometric phases when charge/discharge is stopped, giving the false impression that lithium (de)intercalation is a two-phase process.[221] *In situ* synchrotron X-ray powder diffraction patterns played a central role in identifying the importance of these non-equilibrium phases (**Figure 11a**).

At the same time there is an increasing realisation of the importance of exploiting multiple experimental and computational approaches to develop realistic atomic-scale models of compositionally- and structurally-complex cathode materials. A recent study of the $Li_xMn_{2-x}O_{2-y}F_y$ disordered rocksalt family serves as a topical example. In Ref. 222, Lun and co-workers draw together X-ray and electron diffraction, neutron total scattering, ^{19}F NMR, electron microscopy, voltammetry, X-ray absorption spectroscopy, density functional theory calculations, and Monte Carlo simulations to characterise the local Li, Mn, O, and F arrangements as a function of composition and then to link these distributions to charge capacity. Combinatorial studies such as this currently rely on *ex situ* measurements — often employing different cell environments; ideally each measurement would be performed under identical conditions.

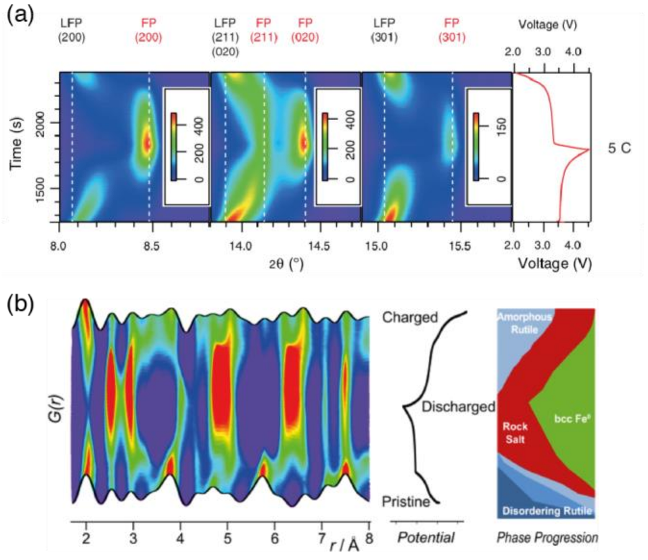

Figure 11. *In Situ* XRD and *operando* PDF measurements. a) *In situ* XRD pattern during fast cycling between $LiFePO_4$ (LFP) and $FePO_4$ (FP). The electrochemical reaction proceeds *via*

an intermediate solid solution, which is evident in the diffraction pattern between the LFP and FP states. Dashed lines indicate the peak positions of the $LiFePO_4$ and $FePO_4$ phases.[221] From [H. Liu, F.C. Strobridge, O.J. Borkiewicz, K.M. Wiaderek, K.W. Chapman, P.J. Chupas, and C.P. Grey, Science 344, 1252817 (2014).] Reprinted with permission from AAAS. b) *Operando* PDF data during charge and discharge for an iron oxyfluoride electrode (left); evolution of Fe phases during cycling (right) determined from analysis of *operando* PDF data.[223] Reprinted with permission from (K.M. Wiaderek, O.J. Borkiewicz, E. Castillo-Martínez, R. Robert, N. Pereira, G.G. Amatucci, C.P. Grey, P.J. Chupas, and K.W. Chapman, Journal of the American Chemical Society 135, 4070). Copyright (2013) American Chemical Society.

Complete structural characterisation of disordered cathodes involves understanding lithium insertion/extraction mechanisms, which in turn requires determining how charge state affects both atomic structure within individual cathode materials, and also the relative amounts of different phases. The ubiquity of amorphous and nanoparticulate phases is a clear challenge in this regard, demanding the use of local probes to identify intermediate phases and track their evolution. For example, *operando* X-ray PDF data have been used to identify the different phases present in an iron oxyfluoride electrode during cycling, and then to determine the corresponding phase fractions as a function of lithium content (**Figure 11b**).[223] The PDF analysis, in combination with *ex situ* NMR showed that the structure of the recharged electrode is different to that of the pristine electrode, even though the discharge capacity is nearly fully recovered upon recharge. The recharged electrode is a complex mixture, comprised of an oxide-rich rocksalt phase and fluoride-rich rutile phase. Despite this mechanistic insight, it is still difficult to determine accurate three-dimensional models of the structures of such complex mixtures.

What is becoming increasingly clear is that very rich crystallographic information is required to develop such models for disordered materials. This insight comes from the use of single-crystal diffuse scattering measurements (either X-ray or neutron) of disordered cathode materials that have revealed the presence of highly-structured scattering that is extremely difficult to measure in powder samples. In the case of Prussian blue analogues, for example, this scattering characterizes the disordered vacancy networks — these dictate the mass transport pathways (**Figure 12a**).[224] Likewise in disordered rocksalts, where the non-random arrangements of transition-metal ions give rise to qualitatively similar scattering.[225] In both cases, there appears to be scope to design and engineer defect networks with specific storage or transport properties. However, the characterisation of these disordered networks appears to rely heavily on access to 3D data sets. Since functioning cathode materials are almost universally obtained in powder form, *in situ* and *operando* measurements give one-dimensional data only: a clear challenge to be addressed.

From an experiment design viewpoint, a parallel ongoing challenge is to ensure that complementary *operando* measurements are meaningfully related. Despite best efforts, *operando* and *in situ* experimental setups are never perfect and the physical region being probed in any one measurement is not necessarily indicative of the cathode as a whole.[216] As a consequence, due care must be taken when interpreting measurements, perhaps increasingly exploiting computational approaches to draw together measurements that pertain to different length scales. An additional complexity is the relevance of cathode history at the time a given measurement was taken. These various considerations form a significant part of the impetus for developing multiprobe measurement capability.

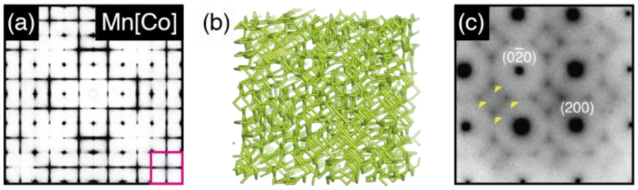

Figure 12. Single-crystal diffuse scattering measurements of disordered cathodes. a) Reconstructed single-crystal diffuse scattering for Mn[Co] Prussian blue analogue in the (hk0) scattering plane; the bottom-right corner is the averaged diffuse scattering patter in the (hk0) plane. b) Representative pore network for the Mn[Co] Prussian blue analogue in (a), determined from Monte Carlo simulation.[224] c) Experimental electron diffraction pattern of $Li_{1.2}Mn_{0.4}Zr_{0.4}O_2$ (LMZO) along the zone axis (100). Reproduced from Ref. 225 [Ji, Urban, Kitchaev, Kwon, Artrith, Ophus, Huang, Cai, Shi, Kim, Kim, and Ceder, Nature Communications (2019)] under Creative Commons Attribution CC BY 4.0.

A good example of such technique development is the combination of *operando* X-ray diffraction and X-ray absorption spectroscopy possible at the B18 beamline at the Diamond Light Source (UK). This beamline has been used, for example, to study long- and short-range structure and electrochemical behavior of a $NiFe_2O_4$/carbon nanotube composite.[226] The bridge to mesoscopic lengthscales seems all the more tractable given the development of X-ray diffraction computed tomography (XRD-CT). By collecting diffraction patterns for a sample in a large number of different orientations and positions, it is possible to obtain a three-dimensional map of diffraction patterns at some fundamental resolution. XRD-CT can track microstructural changes *in situ* whilst providing a spatially resolved picture of the sample, without the need for a specially designed battery cell.[227] Moreover, this approach has even been extended to PDF computed tomography, which allows the short-range structure and spatial distribution of disordered/complex phases to be determined in a single mixture.[228]

With continually developing experimental techniques and the increasing efficiency with which data can be collected for complex multicomponent systems — including cathodes — there is a growing need for multivariate data analysis techniques that can deconvolute these data sets. Multivariate techniques aim to describe a collection of experimental measurements in terms of fewer components. Principal component analysis (PCA) is perhaps the mostly widely used multivariate technique and has been applied to PDF data obtained for battery materials;[223,229] however the difficulty of interpreting PCA analyses of experimental measurements, including PDFs, is well recognised.[229] An important development is the application of novel analysis approaches — including non-negative matrix factorization (NMF) — to the interpretation of complex data sets.[230] Our own experience is that NMF can help characterize otherwise unexpected intermediates that arise during cathode cycling — without *a priori* knowledge of their composition or structure.

Finally, as characterisation techniques for disordered cathodes develop, it is important that these techniques dovetail with advances in computation. Disordered cathodes are complex, dynamic, multicomponent systems and so atomistic models are necessarily large. Here, machine learning approaches are helping develop effective potentials with the accuracy of *ab initio* calculations. The reduction in computational expense is dramatic, giving access to large configurations that capture quantitatively both structure and dynamics as probed experimentally (**Figure 13**).[231]

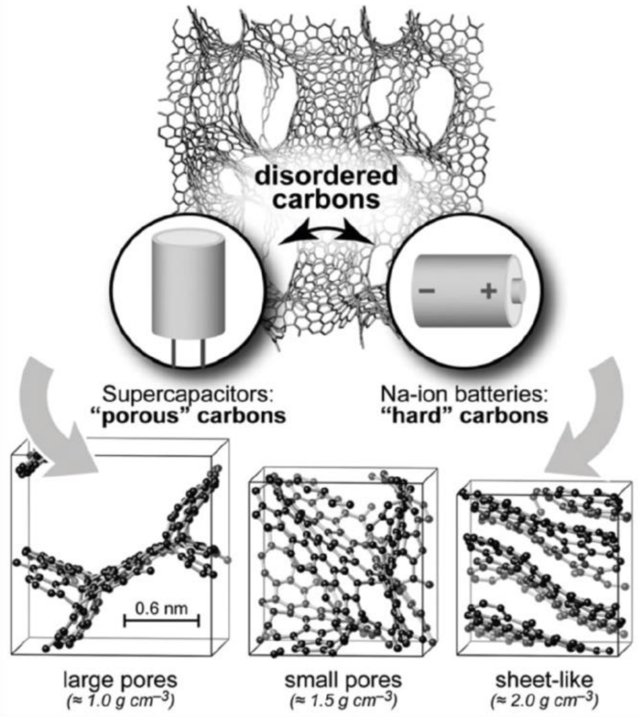

Figure 13. Machine learning approaches for modelling disordered cathodes. Examples of pore structures in disordered carbons, determined from a combination of machine learning and DFT.[231] Different pore sizes are seen experimentally and are each suited to different applications. [V.L. Deringer, C. Merlet, Y. Hu, T.H. Lee, J.A. Kattirtzi, O. Pecher, G. Csányi, S.R. Elliott, and C.P. Grey, Chemical Communications 54, 5988 (2018)] - Published by The Royal Society of Chemistry, reproduced under Creative Commons Attribution CC BY 3.0.

Concluding remarks

We are fortunate that, as our appreciation for the compositional and structural complexity of cathode materials matures, so too is it that the tools used in their characterisation — experimental, analytical, and computational alike — are also developing extremely quickly. That ultimate goal seems ever closer: namely, of developing self-consistent spatially-resolved multi-scale models of cathode materials and their variation during battery operation. This represents no small challenge. Not only are cathodes comprised of multiple components, but those components may be nanoparticulate or amorphous; even the crystalline phases often contain non-trivial compositional or structural disorder. Not only are the materials complex, but so too are the datasets obtained during experimental measurements. For this reason we attach particular weight to the importance of developing robust data analytical methodologies — such as NMF — that allow this complexity to be reduced in a systematic and model-independent fashion.

iii. Establishing Diffusion Properties

John M. Griffin, Innes McClelland, Serena A. Corr and Peter J. Baker

Key to the function of insertion-type cathode materials, especially for high power performance, is the migration of ions through the solid-state structure. In general, diffusion processes within the solid cathode material are significantly slower than liquid-state diffusion in the electrolyte. Therefore, in the development and optimization of cathode materials, it is important to be able to quantify and understand the solid-state diffusion processes that govern charge and discharge mechanisms.

Some of the most well-established methods for quantifying solid-state diffusion are based on electrochemical measurements such as electrochemical impedance spectroscopy (EIS), [232,233] and galvanostatic intermittent titration technique (GITT).[234] These techniques have the advantage that they can be carried out using standard electrochemical equipment and directly relate the ion diffusion to the measured current and voltage. However, they also rely on some assumptions about the structure and properties of the electrochemical cell, which must be modelled as an equivalent circuit in order for the diffusion coefficient to be extracted.

An alternative approach to studying solid-state ion diffusion is to utilize a direct structural probe which is sensitive to ionic motion. One such technique is nuclear magnetic resonance (NMR) which is sensitive to solid-state dynamics over a wide range of timescales. Ionic motion on the millisecond – microsecond timescale can be investigated and quantified through two-dimensional exchange experiments[235] or changes in the position or shape of spectral resonances due to motional averaging of magnetic interactions. Faster nanosecond timescale processes can be quantified by measuring changes in the longitudinal spin relaxation time which is sensitive to fluctuations of the local magnetic field on the timescale of the Larmor frequency (*i.e.*, $\sim 10^9$ s^{-1}).[236]

Another complementary approach is muon spin relaxation (μSR),[237] which measures the spin polarization of muons implanted into the material of interest via the detection of their positron decay products. In systems where ion dynamics are present on the microsecond timescale, they cause fluctuations of the local magnetic field experienced by the muon modulating the spin polarization, which can be interpreted in terms of a rate constant for the ion hopping process.

From both NMR and μSR, the diffusion coefficient is not obtained directly, but can be determined from the precise rate constant for ion hopping that is obtained. Furthermore, variable-temperature measurements of the rate constant enable an activation energy to be obtained for the dynamic process. This can then be correlated with *e.g.*, diffraction structures and theoretical simulations to determine ion migration pathways.

As efforts continue to increase the capacity and decrease the cost of the cathode, it remains important to ensure that new materials retain a high diffusion rate throughout the accessible charge window. This relies on understanding processes ranging from atomic scale hopping between sites, through grain boundaries and interfaces within the particles, to the interfaces formed with the electrolyte, all as a function of the charge state of the cathode.

At the atomic scale, recent measurements have started to uncover how different ion hopping processes can occur within the same material. One of the early kinetic Monte Carlo studies of $LiCoO_2$[238] identified two hopping mechanisms, Tetrahedral Site Hop (TSH) and Oxygen Dumbbell Hop (ODH), with the latter having a larger energy barrier to motion. The presence of two distinct process in Ni-rich NCA materials has recently been identified with ex-situ μSR measurements,[239] with a four-fold difference in energy barriers in excellent agreement with the prediction. The lower-energy barrier process is less clearly evident in $LiCoO_2$ and lower Ni-content materials. An open question is whether particular transition metal combinations act to favour the TSH process and thereby improve the diffusion properties at the atomic scale.

Another area where further understanding can be derived at the atomic level is in cathode phases that only form during the charging or discharging process. The development of *operando* cells for NMR and μSR allow these to be investigated. Questions that are relevant in this area are often related to the structure including accessible pathways and distortions on changing site occupancy.

Understanding motion at grain boundaries and interfaces is considerably more challenging since they represent small volumes within the cell or material, but can be the dominant restrictions on the motion of ions within a cell. There are two approaches to this challenge. Since bulk probes like impedance spectroscopy are sensitive to the greatest restrictions to motion within the cell, differences with the results of local probe measurements are likely to be due to grain boundaries or interfaces. The alternative is to artificially expose or replicate the interface to use surface sensitive local probes, appropriate for controlled interfaces such as those in core-shell nanoparticles, or increasing its size to increase signal contribution, which can work for cathode-electrolyte interfaces.

Since individual probes of diffusion are generally unable to obtain a full picture of a material or its behaviour within a cell, it is vital to combine multiple techniques within a study, and also use theoretical modelling to understand how different pieces of information reflect the full picture.

In situ and *operando* measurements with local probes are well-suited to coupling with techniques that provide bulk measurements; for instance where impedance spectroscopy can be carried out at the same time. Developments in this area will focus on improving the signal from *in situ* cells and enabling faster *operando* measurements.

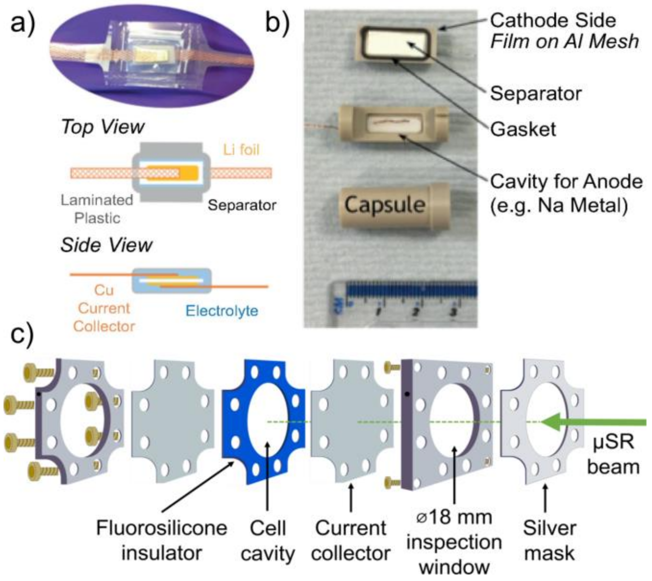

Figure 14. a) NMR bag cell. b) NMR capsule cell. [Adapted from Ref. 240. Copyright 2017 American Chemical Society] under Creative Commons CC BY 4.0 c) μSR cell.

For NMR spectroscopy a number of *in situ* cell designs exist, with the plastic bag cell and plastic capsule cells being the most popular (**Figure 14a and b**). These cells are based on a conventional layered battery structure, but are adapted to fit within the ~10 mm diameter NMR detection coil and also feature mesh current collectors to allow penetration of radiofrequency pulses into the sample.[240] An ongoing challenge is to make these cell designs compatible with variable-temperature conditions whilst maintaining sufficient signal sensitivity and battery performance.

For μSR *in situ* cells are at an earlier stage in their development but are already being applied to questions in cathodes and solid-state electrolytes.[241] Similar to the neutron diffraction cell described above, the coin cell design is ideally suited to the experimental geometry (**Figure 14c**). Specific layers in the cell can be investigated through control of the muon implantation depth and choice of the layer thicknesses. Advantages over NMR include the ability to use different metal foils as current collectors and the ease of variable temperature measurements, although the cell itself needs to be larger to optimise the signal.

Diffusion measurements on novel cathode materials need to work hand-in-hand with theoretical modelling to maximise the information derived from them. Further work on specific materials to identify diffusion pathways, estimate energy barriers, and understand defects will improve the understanding of new materials. More general questions about how the ionic motion affects the probes used to investigate it may also be able to increase the information derived from particular experiments, whether that is in terms of how correlated the ionic motion is, or whether different pathways can be better distinguished in the data.

Concluding remarks

Consistent measurements of diffusion using multiple techniques are now well-established and ready for use in understanding new cathode materials. However, a key consideration is that the choice of technique will necessarily depend on the material properties and the relevant diffusion timescales. Recent work combining multiple techniques has provided a more complete picture of how ions move on different length and time scales in materials.

In situ and *operando* measurements with local probes are developing rapidly to probe materials at intermediate stages of charge but challenges remain in optimizing the cell design, and ensuring that the cells compatible with these techniques provide a realistic model of commercial cells.

Finally, as the theoretical and experimental understanding of diffusion in cathode materials improves, this information can hopefully be used to inform rational materials design, among the numerous other inputs to that process.

iv. Understanding the Interplay between Morphology and Performance

Laura Wheatcroft and Beverley J. Inkson

Greater understanding of complex degradation processes, morphologies, and morphology changes in high energy density cathode materials has required the use of advanced microscopy techniques. **Figure 15** outlines various electron, ion-beam, and X-ray microscopy techniques used in Li-ion battery research, highlighting their lateral resolutions, and typical electrode morphology features which lie within the respective length scales. Depth resolution has also been highlighted for surface sensitive techniques.

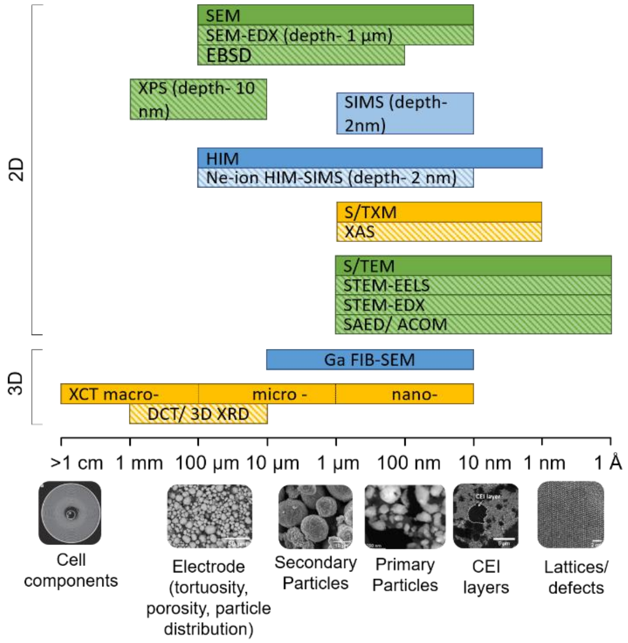

Figure 15. Lateral resolution of different electron (green), ion beam (blue), and X-ray microscopy (yellow) techniques compared with standard cathode morphology

components.[242,243] Solid colours represent microscopy techniques, with striped colours representing the associated chemical or structural characterisation techniques. Electron microscopies represented: scanning electron microscopy (SEM), energy dispersive X-ray spectroscopy (EDX), electron backscatter diffraction (EBSD), X-ray photoelectron spectroscopy (XPS), scanning/ transmission electron microscopy (S/TEM), electron energy loss spectroscopy (EELS), selected area electron diffraction (SAED) and automated crystal orientation mapping (ACOM). Ion-beam microscopies represented: Secondary ion mass spectrometry (SIMS), Helium ion microscopy (HIM), HIM-SIMS, and gallium ion focused ion beam scanning electron microscopy (Ga FIB-SEM). X-ray microscopies represented: Scanning/ transmission X-ray microscopy (S/ TXM), X-ray absorption spectroscopy (XAS), X-ray computed tomography (XCT), Diffraction computed tomography (DCT) and 3D X-ray diffraction (3D XRD). Cell components XCT image reproduced from Ref. 244 [Finegan, Scheel, Robinson, Tjaden, Hunt, Mason, Millichamp, Michiel, Offer, Hinds, Brett, and Shearing, Nature Communications (2015)] under Creative Commons Attribution CC BY 4.0. CEI layer image reproduced from Ref. 245 [Wheatcroft, Klingner, Heller, Hlawacek, Ozkaya, Cookson, and Inkson, ACS Applied Energy Materials (2020)] under Creative Commons Attribution CC BY 4.0.

Recent advances in technique development of some of the techniques outlined in **Figure 15** have led to improved resolution of different electrode features. Some of the recent developments in resolution, and correlation with chemical or structural techniques are highlighted here.

XCT has been widely used for imaging the 3D structure of electrodes. However, segmenting the carbon/ binder domain (CBD) from pores is challenging due to the low attenuation coefficient of the CBD.[246] Recently however, methods to differentiate pores from binder have been developed to overcome this challenge. Contrast between CBD and pores has been enabled by correlating FIB-SEM imaging of CBD-rich regions with XCT,[247] nano-CT of CBD phases with micro-CT,[248] and by using contrast enhancing nanoparticles in the CBD.[249] Accurate analysis of porosity could greatly improve understanding of electrolyte penetration into electrodes, and consequent optimization of electrode structures.

Understanding surface layers, and how underlying morphology effects their growth is important for degradation studies. EBSD has recently been applied to lithium ion battery electrodes to understand grain boundary orientations on electrode surfaces.[250,251] Electrode EBSD has potential applications for understanding preferential lithiation, and CEI growth on different electrode regions. The importance of local environment on CEI growth has also led to CEI characterization using region-of-interest SIMS chemical mapping,[252,253] and HIM-SIMS.[245] Both techniques provide chemical, positional, and thickness information, but the quantification of thickness can be challenging.

Overall, there have been a number of developments in imaging electrode microstructures which aid understanding of degradation processes and improved microstructure development.

A major challenge for cathode microscopy techniques is the development of *in situ* and *operando* techniques. The previous section demonstrated the versatility of microscopy techniques for characterizing electrode morphology. *In situ* and *operando* techniques are beneficial as they enable characterization of transient phenomena and reduce atmosphere induced sample damage. The goal here is to characterize the material in its precise environment as found in a bulk cell. As with the previously examined techniques, *in situ* imaging techniques should aim to be representative of the real cell, and minimize technique induced sample damage.

Ideally the materials used in the real cell should be used in any *operando* characterization. However, the ultra-high vacuum requirements of electron, ion beam, and soft X-ray microscopy limits the choice of electrolyte. Typical organic electrolytes (such as LP-30) are unstable under high vacuum, hence *operando* cells which require electrolyte exposure to the vacuum are limited to ionic liquid and solid-state electrolytes.[254,255]

The geometry of *operando* cell set-ups for nano-scale microscopy (S/TEM, and some S/TXM) can potentially alter diffusion pathways, and make quantitative electrochemistry challenging.[256] Due to the requirement for micro-patterning, Pt electrodes are often used as quasi-reference electrodes however these may cause measured or applied potentials to drift.[256,257] Nano-wire architectures are also used with a solid-electrolyte which can adjust diffusion pathways.[254] Similarly, surface sensitive techniques, such as SEM, SIMS, and XPS cannot use traditional electrodes due to surface sensitive imaging requirements.

Beam damage is a major issue that must be mitigated for all microscopy techniques. X-rays do not typically affect cathode materials, but the incident X-ray beam can cause heating of the electrolyte, and subsequent bubble formation. For electron and ion beam microscopies, heating is also an issue, but radiolysis (particularly in high energy S/TEM) can cause beam induced precipitation in the electrolyte due to reduction by the incident electrons.[258]

A number of strategies have been developed to overcome the vacuum requirements of electron and ion beam microscopy experiments. Electron microscopy in situ cell designs can be classified as open cell, where the components are exposed to high vacuum, and closed-cell where the components are sealed from the vacuum allowing non-vacuum stable electrolytes to be used. The different open- and closed-cell designs for SEM and TEM experiments are detailed in **Figure 16**.

Open-cell designs (**Figure 16a, b, d and e**) consist of cells using high vapour pressure electrolytes, such as ionic liquids,[254,255] and solid-state battery set-ups often prepared by thin-film deposition techniques and FIB sectioning.[259] Open cell set-ups allow for low beam doses to avoid beam damage to organic liquid electrolytes,[258] also, open cells experience no impact on resolution through thickness issues, thus image quality is not compromised. Solid-state battery set-ups have been used for high-resolution interfacial studies, and EELS oxidation state mapping in the TEM.[259] Use of a metal grid with an ionic liquid cell electrolyte has enabled surface sensitive analysis with techniques such as SEM.[255,260] Ionic liquids have also enabled *in situ* XPS experiments.[261]

Closed-cells are designed using electron transparent windows, such as SiN_x, to seal the electrolyte away from the vacuum, enabling the use of standard electrolytes (**Figure 16c, f and g**). Closed-cells have been developed for both SEM, and TEM based experiments, studying the lithiation mechanisms of $LiFePO_4$ with energy filtered TEM,[262] and Li dendrite formation in SEM.[263]

In situ TEM cells require unusual closed-cell geometries due to electron transparency requirements (**Figure 16f**). Recently, a lithium-gold alloy has been reported [257] as a more stable reference electrode than Pt which relies on Li^+ ions from the electrolyte.[264] A sandwich cell with a Li metal anode has also been designed (**Figure 16g**), but the cell relies on exposed nano-rods at the edges for electron transparency.[265]

Luckily, hard X-ray experiments do not have the same vacuum limitations as experienced in electron microscopy. Here, *operando* X-ray microscopy cell geometries can mimic real cells, such as Swagelok set-ups, or coin cells containing kapton windows for X-ray transparency.[266,267]

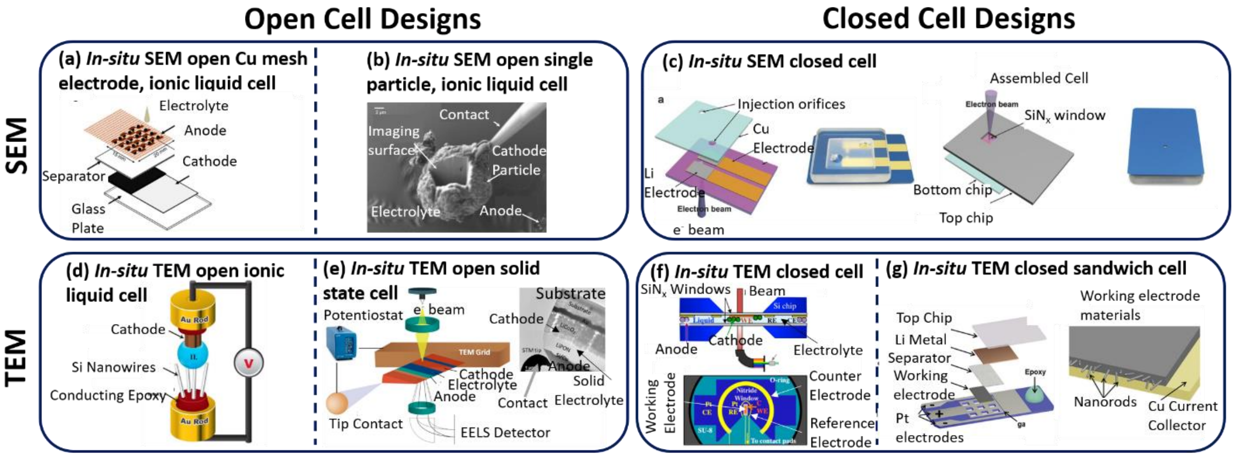

Figure 16. Examples of open and closed cell i*n-situ* TEM and SEM designs. a) Open cell *in-situ* SEM cell design consisting of active material particles on a copper mesh in a sandwich cell geometry with an ionic liquid electrolyte, reproduced from Ref. 255 [Chen, Sano, Tsuda, Ui, Oshima, Yamagata, Ishikawa, Haruta, Doi, Inaba, and Kuwabata, Scientific Reports (2016)] under Creative Commons Attribution CC BY 4.0. b) open cell *in-situ* SEM cell with an active material particle cathode suspended on an ionic liquid electrolyte and lithium titanate anode,[268] (Miller, Proff, Wen, Abraham, and Bareño, Advanced Energy Materials) Copyright © 2013 WILEY-VCH Verlag GmbH & Co. KGaA, Weinheim. c) closed cell *in-situ* SEM design utilising SiN_x observation windows,[263] (Rong, Zhang, Zhao, Qiu, Liu, Ye, Xu, Chen, Hou, Li, Duan, and Zhang, Advanced Materials) © 2017 WILEY-VCH Verlag GmbH & Co. KGaA, Weinheim. d) open cell *in-situ* TEM cell using Si nanowires and an ionic liquid electrolyte,[254] reprinted with permission from (Gu, Parent, Mehdi, Unocic, McDowell, Sacci, Xu, Connell, Xu, Abellan, Chen, Zhang, Perea, Evans, Lauhon, Zhang, Liu, Browning, Cui, Arslan, and Wang, Nano Letters 13, 6106). Copyright (2013) American Chemical Society. e) open all solid state cell *in-situ* TEM cell created using a FIB sectioning,[259] reprinted with permission from (Wang, Santhanagopalan, Zhang, Wang, Xin, He, Li, Dudney, and Meng, Nano Letters 16, 3760). Copyright (2016) American Chemical Society. f) closed cell *in-situ* TEM cell in a 3 electrode configuration using an organic liquid electrolyte,[262] reprinted with permission from (Holtz, Yu, Gunceler, Gao, Sundararaman, Schwarz, Arias, Abruña,

and Muller, Nano Letters 14, 1453). Copyright (2014) American Chemical Society. g) closed cell *in-situ* TEM cell in a sandwich geometry with a Li metal anode.[265] (Xu, Zhang, Liu, Li, Zhao, Li, Zhang, and Zhang, Small) © 2020 WILEY-VCH Verlag GmbH & Co. KGaA, Weinheim.

Concluding remarks

The development of advanced microscopy techniques is enabling improved resolution of multiple components in the complex 3D structure of lithium ion battery cathodes. The improvements in imaging are already having an impact in optimization of microstructure, and understanding of complex degradation mechanisms. The holy grail for microscopy would be to establish *operando* techniques allowing transient information to be gained without sample damage associated with removal from the cell. Numerous different *in situ* cells have been developed for SEM, TEM, and X-ray microscopy, providing information on morphology, and chemical changes during cycling. Some of the developed techniques, such as solid-state open *in situ* electron microscopy cells, do not severely compromise the capability of the instrument due to beam damage during sampling. However, further developments to *in situ* cell design are required to take full advantage of imaging technique whilst minimizing beam damage, improving cyclability, and without limiting material choice.

11. Cathode Mechanical Strength Properties and Testing

Joe C. Stallard and Norman Fleck

Accurate measurements of the Young's modulus, hardness, fracture strength and fracture toughness of cathode materials provide a basis for numerical models that aim to predict the stress state within cathode particles during electrochemical cycling, and determine the origin of mechanical cracking and mechanical damage.[269,270] To date, mechanical tests have been used to quantify the dependence of mechanical properties upon microstructural features such as grain size and internal porosity,[270,271] with the effect of the state of charge and application of successive charge/discharge cycles upon hardness, modulus and fracture strength also investigated.[273,274]

Experimental techniques used to measure the mechanical properties of cathode materials include indentation testing, biaxial flexure and particle compression. Indentation tests are performed by pressing a pyramid-shaped diamond tip into the sample surface with a specified load. After removal of the indentation tip from the sample surface, the area of the indentation mark left by the indentation tip is used to determine the hardness. The Young's modulus may be calculated from measurements of the contact stiffness between the sample and indentation tip,[275] and measurements of fracture toughness are derived from the lengths of cracks that grow from the corners of indentations made with pyramid-shaped tips.[276] Two methods have been used to characterise the fracture strength of cathode materials: biaxial flexure tests have been performed on macroscopic sintered specimens,[271] and uniaxial compression tests on polycrystalline secondary particles have provided an estimation of secondary particle fracture strength.[274] Together, the testing techniques described above allow for the measurement of mechanical properties within individual primary particles, secondary particles, and macroscopic specimens.

Consider the measured mechanical properties of cathode materials. The Young's modulus, hardness and fracture toughness of polycrystalline $LiNi_{0.5}Mn_{0.3}Co_{0.2}O_2$ secondary particles have been measured as 143±11 GPa, 8.3±1.3 GPa and 0.10±0.03 MPa $m^{1/2}$.[273] The measured fracture strength of NMC111 secondary particles is less than 300 MPa,[274] which is less than 1/30th of their hardness, since a low toughness of about 0.1 MPa $m^{1/2}$ [273] endows the secondary particles with elastic-brittle behaviour. Measurements reported in the literature for the olivine cathode material $LiCoPO_4$[277] and layered $LiCoO_2$[278] inform that their mechanical properties lie within an order of magnitude of those measured for ternary $NMC_{x,y,z}$ samples.

The mechanical properties of NMC secondary particles have been measured as a function of their state of charge and charge-discharge history, revealing that their Young's modulus, hardness, fracture strength and fracture toughness all decrease upon delithiation and as a consequence of electrochemical cycling.[273,274] Finite element simulations suggest that this softening within the secondary particles may decrease the internal stresses that develop within them during electrochemical cycling.[269]

Images of polycrystalline secondary particles from cathodes subjected to electrochemical cycling have revealed the development of fractures within and between primary particles,[268] and dislocation networks are observed in secondary particles subjected to multiple charge/discharge cycles.[270] A full understanding of the origin of softening during delithiation and after cycling is yet to be obtained - softening may arise due to the formation of internal cracks; or alternatively may arise as a consequence of variation in the composition of the primary particles brought about by delithiation or other processes. Experiments that measure the mechanical properties of primary particles or single crystal cathode particles as a function of their state of charge are now needed to provide inputs for models that can determine the cause of softening during delithiation and after the application of multiple charge-discharge cycles.

When examining the influence of cycling on cathode materials, a key property in many current cathode materials, including the atomic lattices of olivine and layered cathode materials is their anisotropy. The anisotropy gives rise to anisotropic strains within the lattices during cycling, yet the effects of the anisotropy upon the mechanical properties of the primary particles are largely unexplored. Recent measurements have shown that the fracture toughness of $LiCoO_2$ primary particles varies depending on the direction of testing relative to the lattice orientation,[278] yet the anisotropic moduli and hardness of the layered and olivine cathode material lattices are yet to be measured at the time of writing. Observations of fracture within primary particles[279] have led to suggestions that mechanical cracking may still occur within single crystal cathode architectures; the characterisation of elastic constants within single crystals of anisotropic cathode materials is now needed to provide inputs to models for the prediction of stresses during electrochemical cycling. Methods have been developed to perform such tests on anisotropic crystals[280] with indentation, and could be applied to olivine and layered cathode materials across a wide range of lithium content.

Methods now exist to measure the toughness, modulus, hardness and fracture strength of cathode secondary particles, and the strain state within the atomic lattice of primary particles has been characterized as a function of the state of charge. Technology has also been developed to characterize and observe the changes in the particle microstructure during cycling. The understanding of mechanical damage within cathode particles remains an important goal for research, and relies upon the development of predictive models that can capture the necessary physics that leads to the development of stress. At the basis of these models lies an assumed relationship between state of charge, diffusivity and mechanical properties.[269]

Early predictions for the stress state within cathode particles during charge and discharge assumed that diffusion could be modelled accurately without consideration of mechanical stresses, and that the stresses simply followed from the distribution of charge and resultant lattice strain. More recently coupled relationships between diffusivity and stress have since been adopted for use in simulation,[269] and the variation of diffusivity with the state of charge has been measured. The variation in cathode material modulus, hardness and toughness with the state of charge remains unaccounted for. At present, assumed relationships between the distribution of stress, state of charge and diffusivity within cathode particles still lack experimental confirmation, and thus present an important opportunity to scientists for experimental study and characterization.

Experimental techniques that measure strains and stresses *in situ* have already been developed to measure the swelling in the porous cathode composite that forms the active material of a lithium-ion cell. Porous cathodes are cast as films upon a foil backing. As the porous cathode structure swells during charge and discharge, the bending of the foil structure allows the strain to be recorded.[281] The cathode layer may also be subjected to an external stress by bending the foil with an applied force. Such experiments allow a combination of mechanical and electrochemical stimuli to be applied to cathodes. With the advent of suitable sample processing techniques that allow for the investigation of single crystal cathode specimens, similar experimental techniques might facilitate characterization of the relationships between mechanical properties and state of charge that are hitherto unknown. Such experiments will rely on new methods for sample preparation, and require mechanical tests of cathode materials to be performed within the cell environment.

Concluding remarks

Mechanical tests have revealed that polycrystalline cathode particles are elastic brittle in tension, and that their modulus, hardness, fracture toughness and fracture strength all vary with electrochemical cycling and their state of charge. It remains to determine the origin of softening upon delithiation and cycling, and to arrive at comprehensive models that can predict the conditions under which cathode particle fracture takes place. Anisotropy in the mechanical properties of primary particles, the variation in their mechanical properties during cycling, and the relationships between the state of charge, diffusivity and mechanical stress are all topics for future experimentation. Test methods exist for the characterization of anisotropic crystals and for pre-charging specimens prior to measurement of their mechanical properties, whereas measurement of the relationships between stress, state of charge and diffusivity may require the development of new experimental techniques that capable of imposing mechanical and electrochemical loads simultaneously.

12. Acknowledgements

This work was supported by the Faraday Institution project FutureCat (grant number FIRG017).

13. References

1 K. Mizushima, P. Jones, P. Wiseman, and J. Goodenough, Solid State Ionics **3-4**, 171 (1981).

2 T. Ohsaki, T. Kishi, T. Kuboki, N. Takami, N. Shimura, Y. Sato, M. Sekino, and A. Satoh, Journal of Power Sources **146**, 97 (2005).

3 N. Yabuuchi and T. Ohzuku, Journal of Power Sources **119-121**, 171 (2003).

4 Y.W. Tsai, B.J. Hwang, G. Ceder, H.S. Sheu, D.G. Liu, and J.F. Lee, Chemistry of Materials **17**, 3191 (2005).

5 N. Yabuuchi, Y. Makimura, and T. Ohzuku, Journal of The Electrochemical Society **154**, 314 (2007).

6 W. Li, E.M. Erickson, and A. Manthiram, Nature Energy **5**, 26 (2020).

7 M. Bianchini, M. Roca-Ayats, P. Hartmann, T. Brezesinski, and J. Janek, **58**, 10434 (2019).

8 M. Bianchini, M. Roca-Ayats, P. Hartmann, T. Brezesinski, and J. Janek, **58**, 10434 (2019).

9 L. Mu, Z. Yang, L. Tao, C.K. Waters, Z. Xu, L. Li, S. Sainio, Y. Du, H.L. Xin, D. Nordlund, and F. Lin, Journal of Materials Chemistry A (2020).

10 F. Lin, I.M. Markus, D. Nordlund, T.-C. Weng, M.D. Asta, H.L. Xin, and M.M. Doeff, Nature Communications **5**, (2014).

11 L. Liang, W. Zhang, F. Zhao, D.K. Denis, F. uz Zaman, L. Hou, and C. Yuan, Advanced Materials Interfaces **7**, 1901749 (2019).

12 Q. Xie, W. Li, and A. Manthiram, Chemistry of Materials **31**, 938 (2019).

13 H. Li, P. Zhou, F. Liu, H. Li, F. Cheng, and J. Chen, Chemical Science **10**, 1374 (2019).

14 M. Guilmard, L. Croguennec, D. Denux, and C. Delmas, Chemistry of Materials **15**, 4476 (2003).

15 U.-H. Kim, D.-W. Jun, K.-J. Park, Q. Zhang, P. Kaghazchi, D. Aurbach, D.T. Major, G. Goobes, M. Dixit, N. Leifer, C.M. Wang, P. Yan, D. Ahn, K.-H. Kim, C.S. Yoon, and Y.-K. Sun, Energy & Environmental Science **11**, 1271 (2018).

16 H.-H. Ryu, G.-T. Park, C.S. Yoon, and Y.-K. Sun, Journal of Materials Chemistry A **7**, 18580 (2019).

17 C.S. Yoon, U.-H. Kim, G.-T. Park, S.J. Kim, K.-H. Kim, J. Kim, and Y.-K. Sun, ACS Energy Letters **3**, 1634 (2018).

18 H. Xie, K. Du, G. Hu, Z. Peng, and Y. Cao, The Journal of Physical Chemistry C **120**, 3235 (2016).

19 M. Chen, E. Zhao, D. Chen, M. Wu, S. Han, Q. Huang, L. Yang, X. Xiao, and Z. Hu, Inorganic Chemistry **56**, 8355 (2017).

20 T. Weigel, F. Schipper, E.M. Erickson, F.A. Susai, B. Markovsky, and D. Aurbach, ACS Energy Letters **4**, 508 (2019).

21 L. Mu, R. Zhang, W.H. Kan, Y. Zhang, L. Li, C. Kuai, B. Zydlewski, M.M. Rahman, C.-J. Sun, S. Sainio, M. Avdeev, D. Nordlund, H.L. Xin, and F. Lin, Chemistry of Materials **31**, 9769 (2019).

22 C. Li, H.P. Zhang, L.J. Fu, H. Liu, Y.P. Wu, E. Rahm, R. Holze, and H.Q. Wu, Electrochimica Acta **51**, 3872 (2006).

23 M.K. Shobana, Journal of Alloys and Compounds **802**, 477 (2019).

24 X. Meng, X.-Q. Yang, and X. Sun, Advanced Materials **24**, 3589 (2012).

25 W. Zhu, X. Huang, T. Liu, Z. Xie, Y. Wang, K. Tian, L. Bu, H. Wang, L. Gao, and J. Zhao, Coatings **9**, 92 (2019).

26 D. Mohanty, K. Dahlberg, D.M. King, L.A. David, A.S. Sefat, D.L. Wood, C. Daniel, S. Dhar, V. Mahajan, M. Lee, and F. Albano, Scientific Reports **6**, (2016).

27 G. Qian, Y. Zhang, L. Li, R. Zhang, J. Xu, Z. Cheng, S. Xie, H. Wang, Q. Rao, Y. He, Y. Shen, L. Chen, M. Tang, and Z.-F. Ma, Energy Storage Materials **27**, 140 (2020).

28 Z. Xu, Z. Jiang, C. Kuai, R. Xu, C. Qin, Y. Zhang, M.M. Rahman, C. Wei, D. Nordlund, C.-J. Sun, X. Xiao, X.-W. Du, K. Zhao, P. Yan, Y. Liu, and F. Lin, Nature Communications **11**, (2020).

29 J. Kim, H. Lee, H. Cha, M. Yoon, M. Park, and J. Cho, Advanced Energy Materials **8**, 1702028 (2017).

30 Y. Kim, ACS Applied Materials & Interfaces **4**, 2329 (2012).

31 X. Fan, G. Hu, B. Zhang, X. Ou, J. Zhang, W. Zhao, H. Jia, L. Zou, P. Li, and Y. Yang, Nano Energy **70**, 104450 (2020).

32 H. Cha, J. Kim, H. Lee, N. Kim, J. Hwang, J. Sung, M. Yoon, K. Kim, and J. Cho, Advanced Materials **32**, 2003040 (2020).

33 Y. Bi, J. Tao, Y. Wu, L. Li, Y. Xu, E. Hu, B. Wu, J. Hu, C. Wang, J.-G. Zhang, Y. Qi, and J. Xiao, Science **370**, 1313 (2020).

34 J. Zhu and G. Chen, Journal of Materials Chemistry A **7**, 5463 (2019).

35 H. Li, J. Li, N. Zaker, N. Zhang, G.A. Botton, and J.R. Dahn, Journal of The Electrochemical Society **166**, 1956 (2019).

36 J. Langdon and A. Manthiram, Energy Storage Materials (2021).

37 T. Ohzuku, S. Takeda, and M. Iwanaga, Journal of Power Sources **81-82**, 90 (1999).

38 S.H. Park, S.-W. Oh, S.H. Kang, I. Belharouak, K. Amine, and Y.-K. Sun, Electrochimica Acta **52**, 7226 (2007).

39 M. Hu, X. Pang, and Z. Zhou, Journal of Power Sources **237**, 229 (2013).

40 J. Song, D.W. Shin, Y. Lu, C.D. Amos, A. Manthiram, and J.B. Goodenough, Chemistry of Materials **24**, 3101 (2012).

41 J.-H. Kim, S.-T. Myung, C.S. Yoon, S.G. Kang, and Y.-K. Sun, Chemistry of Materials **16**, 906 (2004).

42 X. Ma, B. Kang, and G. Ceder, Journal of The Electrochemical Society **157**, 925 (2010).

43 J. Liu, A. Huq, Z. Moorhead-Rosenberg, A. Manthiram, and K. Page, Chemistry of Materials **28**, 6817 (2016).

44 M. Egashira, H. Takahashi, S. Okada, and J.-ichi Yamaki, Journal of Power Sources **92**, 267 (2001).

45 T.-F. Yi, J. Mei, and Y.-R. Zhu, Journal of Power Sources **316**, 85 (2016).

46 M. Moshkovich, M. Cojocaru, H.E. Gottlieb, and D. Aurbach, Journal of Electroanalytical Chemistry **497**, 84 (2001).

47 J.-H. Kim, N.P.W. Pieczonka, and L. Yang, ChemPhysChem **15**, 1940 (2014).

48 X. Cao, X. He, J. Wang, H. Liu, S. Röser, B.R. Rad, M. Evertz, B. Streipert, J. Li, R. Wagner, M. Winter, and I. Cekic-Laskovic, ACS Applied Materials & Interfaces **8**, 25971 (2016).

49 N.P.W. Pieczonka, Z. Liu, P. Lu, K.L. Olson, J. Moote, B.R. Powell, and J.-H. Kim, The Journal of Physical Chemistry C **117**, 15947 (2013).

50 T. Liu, A. Dai, J. Lu, Y. Yuan, Y. Xiao, L. Yu, M. Li, J. Gim, L. Ma, J. Liu, C. Zhan, L. Li, J. Zheng, Y. Ren, T. Wu, R. Shahbazian-Yassar, J. Wen, F. Pan, and K. Amine, Nature Communications **10**, (2019).

51 D.S. Lu, L.B. Yuan, J.L. Li, R.Q. Huang, J.H. Guo, and Y.P. Cai, Journal of Electroanalytical Chemistry **758**, 33 (2015).

52 M. Lin, L. Ben, Y. Sun, H. Wang, Z. Yang, L. Gu, X. Yu, X.-Q. Yang, H. Zhao, R. Yu, M. Armand, and X. Huang, Chemistry of Materials **27**, 292 (2014).

53 K.W. Leitner, H. Wolf, A. Garsuch, F. Chesneau, and M. Schulz-Dobrick, Journal of Power Sources **244**, 548 (2013).

54 O.(Y. Chusid, E.E. Ely, D. Aurbach, M. Babai, and Y. Carmeli, Journal of Power Sources **43**, 47 (1993).

55 G.Q. Liu, L. Wen, X. Wang, and B.Y. Ma, Journal of Alloys and Compounds **509**, 9377 (2011).

56 D.W. Shin, C.A. Bridges, A. Huq, M.P. Paranthaman, and A. Manthiram, Chemistry of Materials **24**, 3720 (2012).

57 G. Fey, Journal of Power Sources **115**, 332 (2003).

58 J.-feng Wang, D. Chen, W. WU, L. WANG, and G.-chuan LIANG, Transactions of Nonferrous Metals Society of China **27**, 2239 (2017).

59 B. Xiao, H. Liu, J. Liu, Q. Sun, B. Wang, K. Kaliyappan, Y. Zhao, M.N. Banis, Y. Liu, R. Li, T.-K. Sham, G.A. Botton, M. Cai, and X. Sun, Advanced Materials **29**, 1703764 (2017).

60 G.B. Zhong, Y.Y. Wang, Y.Q. Yu, and C.H. Chen, Journal of Power Sources **205**, 385 (2012).

61 Y. Luo, H. Li, T. Lu, Y. Zhang, S.S. Mao, Z. Liu, W. Wen, J. Xie, and L. Yan, Electrochimica Acta **238**, 237 (2017).

62 Y. Shu, Y. Xie, W. Yan, S. Meng, D. Sun, Y. Jin, and K. He, Journal of Power Sources **433**, 226708 (2019).

63 J.-H. Kim, N.P.W. Pieczonka, P. Lu, Z. Liu, R. Qiao, W. Yang, M.M. Tessema, Y.-K. Sun, and B.R. Powell, Advanced Materials Interfaces **2**, 1500109 (2015).

64 Q. Xia, X. Zhao, M. Xu, Z. Ding, J. Liu, L. Chen, D.G. Ivey, and W. Wei, Journal of Materials Chemistry A **3**, 3995 (2015).

65 J.F. Liu, Y.F. Chen, J. Xu, W.W. Sun, C.M. Zheng, and Y.J. Li, RSC Advances **9**, 3081 (2019).

66 J. Chong, S. Xun, J. Zhang, X. Song, H. Xie, V. Battaglia, and R. Wang, Chemistry - A European Journal **20**, 7479 (2014).

67 J. Chong, S. Xun, X. Song, G. Liu, and V.S. Battaglia, Nano Energy **2**, 283 (2013).

68 Y. Deng, J. Mou, H. Wu, N. Jiang, Q. Zheng, K.H. Lam, C. Xu, and D. Lin, Electrochimica Acta **235**, 19 (2017).

69 U. Nisar, S.A.J.A. Al-Hail, R.K. Petla, R.A. Shakoor, R. Essehli, R. Kahraman, S.Y. AlQaradawi, D.K. Kim, I. Belharouak, and M.R. Amin, ACS Applied Energy Materials **2**, 7263 (2019).

70 Q. Chang, A. Wei, W. Li, X. Bai, L. Zhang, R. He, and Z. Liu, Ceramics International **45**, 5100 (2019).

71 S. Deng, B. Wang, Y. Yuan, X. Li, Q. Sun, K. Doyle-Davis, M.N. Banis, J. Liang, Y. Zhao, J. Li, R. Li, T.-K. Sham, R. Shahbazian-Yassar, H. Wang, M. Cai, J. Lu, and X. Sun, Nano Energy **65**, 103988 (2019).

72 H. Bouayad, Z. Wang, N. Dupré, R. Dedryvère, D. Foix, S. Franger, J.-F. Martin, L. Boutafa, S. Patoux, D. Gonbeau, and D. Guyomard, The Journal of Physical Chemistry C **118**, 4634 (2014).

73 J.C. Arrebola, A. Caballero, M. Cruz, L. Hernán, J. Morales, and E.R. Castellón, Advanced Functional Materials **16**, 1904 (2006).

74 F. Wu, H. Zhou, Y. Bai, H. Wang, and C. Wu, ACS Applied Materials & Interfaces **7**, 15098 (2015).

75 Y. Abu-Lebdeh and I. Davidson, Journal of Power Sources **189**, 576 (2009).

76 H. Xu, H. Zhang, J. Ma, G. Xu, T. Dong, J. Chen, and G. Cui, ACS Energy Letters **4**, 2871 (2019).

77 J. Wang, Y. Yamada, K. Sodeyama, C.H. Chiang, Y. Tateyama, and A. Yamada, Nature Communications **7**, (2016).

78 Z. Zou, H. Xu, H. Zhang, Y. Tang, and G. Cui, ACS Applied Materials & Interfaces **12**, 21368 (2020).

79 R.J. Clément, Z. Lun, and G. Ceder, Energy & Environmental Science **13**, 345 (2020).

80 K. Kang and G. Ceder, Physical Review B **74**, (2006).

81 A.V. der Ven, J. Bhattacharya, and A.A. Belak, Accounts of Chemical Research **46**, 1216 (2012).

82 V. Pralong, V. Gopal, V. Caignaert, V. Duffort, and B. Raveau, Chemistry of Materials **24**, 12 (2011).

83 N. Yabuuchi, M. Takeuchi, M. Nakayama, H. Shiiba, M. Ogawa, K. Nakayama, T. Ohta, D. Endo, T. Ozaki, T. Inamasu, K. Sato, and S. Komaba, Proceedings of the National Academy of Sciences **112**, 7650 (2015).

84 M. Diaz-Lopez, M. Freire, Y. Joly, C.V. Colin, H.E. Fischer, N. Blanc, N. Boudet, V. Pralong, and P. Bordet, Chemistry of Materials **30**, 3060 (2018).

85 M. Freire, N.V. Kosova, C. Jordy, D. Chateigner, O.I. Lebedev, A. Maignan, and V. Pralong, Nature Materials **15**, 173 (2015).

86 Z. Lun, B. Ouyang, D.H. Kwon, Y. Ha, E.E. Foley, T.Y. Huang, Z. Cai, H. Kim, M. Balasubramanian, Y. Sun, J. Huang, Y. Tian, H. Kim, B.D. McCloskey, W. Yang, R.J. Clément, H. Ji, and G. Ceder, Nat Mater (2020).

87 R. Sharpe, R.A. House, M.J. Clarke, D. Förstermann, J.-J. Marie, G. Cibin, K.-J. Zhou, H.Y. Playford, P.G. Bruce, and M.S. Islam, Journal of the American Chemical Society **142**, 21799 (2020).

88 M. Freire, O.I. Lebedev, A. Maignan, C. Jordy, and V. Pralong, J. Mater. Chem. A **5**, 21898 (2017).

89 M. Diaz-Lopez, P.A. Chater, Y. Joly, O. Proux, J.-L. Hazemann, P. Bordet, and V. Pralong, Journal of Materials Chemistry A **8**, 10998 (2020).

90 M.A. Jones, P.J. Reeves, I.D. Seymour, M.J. Cliffe, S.E. Dutton, and C.P. Grey, Chemical Communications **55**, 9027 (2019).

91 Z.N. Taylor, A.J. Perez, J.A. Coca-Clemente, F. Braga, N.E. Drewett, M.J. Pitcher, W.J. Thomas, M.S. Dyer, C. Collins, M. Zanella, T. Johnson, S. Day, C. Tang, V.R. Dhanak, J.B. Claridge, L.J. Hardwick, and M.J. Rosseinsky, Journal of the American Chemical Society **141**, 7333 (2019).

92 Y. Gao, X. Wang, J. Ma, Z. Wang, and L. Chen, Chemistry of Materials **27**, 3456 (2015).

93 M. Diaz-Lopez, P.A. Chater, P. Bordet, M. Freire, C. Jordy, O.I. Lebedev, and V. Pralong, Advanced Energy Materials **10**, 1902788 (2020).

94 R. Chen, S. Ren, M. Yavuz, A.A. Guda, V. Shapovalov, R. Witter, M. Fichtner, and H. Hahn, Physical Chemistry Chemical Physics **17**, 17288 (2015).

95 B. Ouyang, N. Artrith, Z. Lun, Z. Jadidi, D.A. Kitchaev, H. Ji, A. Urban, and G. Ceder, Advanced Energy Materials **10**, 1903240 (2020).

96 I. Källquist, A.J. Naylor, C. Baur, J. Chable, J. Kullgren, M. Fichtner, K. Edström, D. Brandell, and M. Hahlin, Chemistry of Materials **31**, 6084 (2019).

97 M. Sathiya, G. Rousse, K. Ramesha, C.P. Laisa, H. Vezin, M.T. Sougrati, M.-L. Doublet, D. Foix, D. Gonbeau, W. Walker, A.S. Prakash, M.B. Hassine, L. Dupont, and J.-M. Tarascon, Nature Materials **12**, 827 (2013).

98 M. Saubanère, E. McCalla, J.-M. Tarascon, and M.-L. Doublet, Energy & Environmental Science **9**, 984 (2016).

99 P.E. Pearce, G. Assat, A. Iadecola, F. Fauth, R. Dedryvère, A. Abakumov, G. Rousse, and J.-M. Tarascon, The Journal of Physical Chemistry C **124**, 2771 (2020).

100 E. McCalla, A.M. Abakumov, M. Saubanere, D. Foix, E.J. Berg, G. Rousse, M.-L. Doublet, D. Gonbeau, P. Novak, G.V. Tendeloo, R. Dominko, and J.-M. Tarascon, Science **350**, 1516 (2015).

101 D. Foix, M. Sathiya, E. McCalla, J.-M. Tarascon, and D. Gonbeau, The Journal of Physical Chemistry C **120**, 862 (2016).

102 C.J. Hansen, J.J. Zak, A.J. Martinolich, J.S. Ko, N.H. Bashian, F. Kaboudvand, A.V. der Ven, B.C. Melot, J.N. Weker, and K.A. See, Journal of the American Chemical Society **142**, 6737 (2020).

103 F. Wu and G. Yushin, Energy & Environmental Science **10**, 435 (2017).

104 S.-H. Yu, X. Feng, N. Zhang, J. Seok, and H.D. Abruña, Accounts of Chemical Research **51**, 273 (2018).

105 X. Hua, R. Robert, L.-S. Du, K.M. Wiaderek, M. Leskes, K.W. Chapman, P.J. Chupas, and C.P. Grey, The Journal of Physical Chemistry C **118**, 15169 (2014).

106 X. Fan, E. Hu, X. Ji, Y. Zhu, F. Han, S. Hwang, J. Liu, S. Bak, Z. Ma, T. Gao, S.-C. Liou, J. Bai, X.-Q. Yang, Y. Mo, K. Xu, D. Su, and C. Wang, Nature Communications **9**, (2018).

107 P.G. Bruce, S.A. Freunberger, L.J. Hardwick, and J.-M. Tarascon, Nature Materials **11**, 19 (2011).

108 F. Wu, J. Maier, and Y. Yu, Chemical Society Reviews **49**, 1569 (2020).

109 C. Chen, Y. Zuo, W. Ye, X. Li, Z. Deng, and S.P. Ong, Advanced Energy Materials **10**, 1903242 (2020).

110 M.T. Sougrati, A. Darwiche, X. Liu, A. Mahmoud, R.P. Hermann, S. Jouen, L. Monconduit, R. Dronskowski, and L. Stievano, Angewandte Chemie International Edition **55**, 5090 (2016).

111 H. Zhang, B.M. May, F. Omenya, M.S. Whittingham, J. Cabana, and G. Zhou, Chemistry of Materials **31**, 7790 (2019).

112 S. Sharifi-Asl, J. Lu, K. Amine, and R. Shahbazian-Yassar, Advanced Energy Materials **9**, 1900551 (2019).

113 A. Hammami, N. Raymond, and M. Armand, Nature **424**, 635 (2003).

114 S. Saha, G. Assat, M.T. Sougrati, D. Foix, H. Li, J. Vergnet, S. Turi, Y. Ha, W. Yang, J. Cabana, G. Rousse, A.M. Abakumov, and J.-M. Tarascon, Nature Energy **4**, 977 (2019).

115 J. Cabana, L. Monconduit, D. Larcher, and M.R. Palacín, Advanced Materials **22**, 170 (2010).

116 F. Badway, F. Cosandey, N. Pereira, and G.G. Amatucci, Journal of The Electrochemical Society **150**, 1318 (2003).

117 A.R. Armstrong and P.G. Bruce, Nature **381**, 499 (1996).

118 E.A. Olivetti, G. Ceder, G.G. Gaustad, and X. Fu, Joule **1**, 229 (2017).

119 B. Simon, S. Ziemann, and M. Weil, Resources Conservation and Recycling **104**, 300 (2015).

120 J. Lee, J.K. Papp, R.J. Clément, S. Sallis, D.-H. Kwon, T. Shi, W. Yang, B.D. McCloskey, and G. Ceder, Nature Communications **8**, (2017).

121 W. Lee, S. Muhammad, C. Sergey, H. Lee, J. Yoon, Y.-M. Kang, and W.-S. Yoon, Angewandte Chemie International Edition **59**, 2578 (2020).

122 K.T. Lai, I. Antonyshyn, Y. Prots, and M. Valldor, Journal of the American Chemical Society **139**, 9645 (2017).

123 D. Mikhailova, L. Giebeler, S. Maletti, S. Oswald, A. Sarapulova, S. Indris, Z. Hu, J. Bednarcik, and M. Valldor, ACS Applied Energy Materials **1**, 6593 (2018).

124 Z. Lu and F. Ciucci, Journal of Materials Chemistry A **6**, 5185 (2018).

125 T. Matsumura, R. Kanno, Y. Inaba, Y. Kawamoto, and M. Takano, Journal of The Electrochemical Society **149**, 1509 (2002).

126 S.-H. Wu and H.-Y. Liu, Journal of Power Sources **174**, 789 (2007).

127 M.A. Hayward, M.A. Green, M.J. Rosseinsky, and J. Sloan, Journal of the American Chemical Society **121**, 8843 (1999).

128 A. Manthiram, Nature Communications **11**, (2020).

129 A.D. Becke, The Journal of Chemical Physics **140**, 18 (2014).

130 A.R. Oganov, C.J. Pickard, Q. Zhu, and R.J. Needs, Nature Reviews Materials **4**, 331 (2019).

131 H. Guo, H. Ping, J. Hu, X. Song, J. Zheng, and F. Pan, Journal of Materials Chemistry A **5**, 14294 (2017).

132 X. Zhao, S. Wu, X. Lv, M.C. Nguyen, C.-Z. Wang, Z. Lin, Z.-Z. Zhu, and K.-M. Ho, Scientific Reports **5**, (2015).

133 G. Hautier, C. Fischer, V. Ehrlacher, A. Jain, and G. Ceder, Inorganic Chemistry **50**, 656 (2011).

134 D.J. Wales and J.P.K. Doye, The Journal of Physical Chemistry A **101**, 5111 (1997).

135 S. Goedecker, The Journal of Chemical Physics **120**, 9911 (2004).

136 A.R. Oganov, C.W. Glass, and S. Ono, Earth and Planetary Science Letters **241**, 95 (2006).

137 Y. Wang, J. Lv, L. Zhu, and Y. Ma, Computer Physics Communications **183**, 2063 (2012).

138 C.J. Pickard and R.J. Needs, Physical Review Letters **97**, (2006).

139 C.J. Pickard and R.J. Needs, Journal of Physics: Condensed Matter **23**, 053201 (2011).

140 R.J. Nicholls, N. Ni, S. Lozano-Perez, A. London, D.W. McComb, P.D. Nellist, C.R.M. Grovenor, C.J. Pickard, and J.R. Yates, Advanced Engineering Materials **17**, 211 (2014).

141 S.L. Dudarev, G.A. Botton, S.Y. Savrasov, C.J. Humphreys, and A.P. Sutton, Physical Review B **57**, 1505 (1998).

142 A.V. Krukau, O.A. Vydrov, A.F. Izmaylov, and G.E. Scuseria, The Journal of Chemical Physics **125**, 224106 (2006).

143 D.W. Davies, K.T. Butler, A.J. Jackson, A. Morris, J.M. Frost, J.M. Skelton, and A. Walsh, Chem **1**, 617 (2016).

144 E.B. Isaacs, S. Patel, and C. Wolverton, Physical Review Materials **4**, (2020).

145 J. Sun, A. Ruzsinszky, and J.P. Perdew, Physical Review Letters **115**, (2015).

146 J. Behler and M. Parrinello, Physical Review Letters **98**, (2007).

147 A.P. Bartók, M.C. Payne, R. Kondor, and G. Csányi, Physical Review Letters **104**, (2010).

148 V.L. Deringer, D.M. Proserpio, G. Csányi, and C.J. Pickard, Faraday Discussions **211**, 45 (2018).

149 B. Cheng, R.-R. Griffiths, S. Wengert, C. Kunkel, T. Stenczel, B. Zhu, V.L. Deringer, N. Bernstein, J.T. Margraf, K. Reuter, and G. Csanyi, Accounts of Chemical Research (2020).

150 A. Jain, S.P. Ong, G. Hautier, W. Chen, W.D. Richards, S. Dacek, S. Cholia, D. Gunter, D. Skinner, G. Ceder, and K.A. Persson, APL Materials **1**, 011002 (2013).

151 S. Kirklin, J.E. Saal, B. Meredig, A. Thompson, J.W. Doak, M. Aykol, S. Rühl, and C. Wolverton, Npj Computational Materials **1**, (2015).

152 C. Chen, W. Ye, Y. Zuo, C. Zheng, and S.P. Ong, Chemistry of Materials **31**, 3564 (2019).

153 D.W. Davies, B.J. Morgan, D.O. Scanlon, and A. Walsh, IOP SciNotes **1**, 024805 (2020).

154 J. Zheng, Y. Ye, and F. Pan, National Science Review **7**, 242 (2019).

155 P. Hou, H. Zhang, Z. Zi, L. Zhang, and X. Xu, Journal of Materials Chemistry A **5**, 4254 (2017).

156 A. van Bommel and J.R. Dahn, Chemistry of Materials **21**, 1500 (2009).

157 M.-H. Lee, Y.-J. Kang, S.-T. Myung, and Y.-K. Sun, Electrochimica Acta **50**, 939 (2004).

158 F. Zhou, X. Zhao, A. van Bommel, A.W. Rowe, and J.R. Dahn, Chemistry of Materials **22**, 1015 (2010).

159 Y.-K. Sun, S.-T. Myung, M.-H. Kim, J. Prakash, and K. Amine, Journal of the American Chemical Society **127**, 13411 (2005).

160 L. Liang, X. Sun, C. Wu, L. Hou, J. Sun, X. Zhang, and C. Yuan, ACS Applied Materials & Interfaces **10**, 5498 (2018).

161 X. Dong, J. Yao, W. Zhu, X. Huang, X. Kuai, J. Tang, X. Li, S. Dai, L. Shen, R. Yang, L. Gao, and J. Zhao, Journal of Materials Chemistry A **7**, 20262 (2019).

162 P. Hou, J. Guo, D. Song, J. Zhang, E. Zhou, and L. Zhang, Chemistry Letters **41**, 1712 (2012).

163 Y.-K. Sun, S.-T. Myung, B.-C. Park, J. Prakash, I. Belharouak, and K. Amine, Nature Materials **8**, 320 (2009).

164 Y.-K. Sun, Z. Chen, H.-J. Noh, D.-J. Lee, H.-G. Jung, Y. Ren, S. Wang, C.S. Yoon, S.-T. Myung, and K. Amine, Nature Materials **11**, 942 (2012).

165 B.-B. Lim, S.-J. Yoon, K.-J. Park, C.S. Yoon, S.-J. Kim, J.J. Lee, and Y.-K. Sun, Advanced Functional Materials **25**, 4673 (2015).

166 D. Song, P. Hou, X. Wang, X. Shi, and L. Zhang, ACS Applied Materials & Interfaces **7**, 12864 (2015).

167 C. Xu, K. Märker, J. Lee, A. Mahadevegowda, P.J. Reeves, S.J. Day, M.F. Groh, S.P. Emge, C. Ducati, B.L. Mehdi, C.C. Tang, and C.P. Grey, Nature Materials **20**, 84 (2020).

168 R.J. Mou and K.P.C. Yao, Journal of the Electrochemical Society **168**, 020503 (2021).

169 M. Park, X. Zhang, M. Chung, G.B. Less, and A.M. Sastry, Journal of Power Sources **195**, 7904 (2010).

170 Y.-H. Chen, C.-W. Wang, X. Zhang, and A.M. Sastry, Journal of Power Sources **195**, 2851 (2010).

171 B.L. Trembacki, A.N. Mistry, D.R. Noble, M.E. Ferraro, P.P. Mukherjee, and S.A. Roberts, Journal of The Electrochemical Society **165**, 725 (2018).

172 G. Inoue and M. Kawase, Journal of Power Sources **342**, 476 (2017).

173 Q. Cao, H.P. Zhang, G.J. Wang, Q. Xia, Y.P. Wu, and H.Q. Wu, Electrochemistry Communications **9**, 1228 (2007).

174 J. Kim, B. Kim, J.-G. Lee, J. Cho, and B. Park, Journal of Power Sources **139**, 289 (2005).

175 H.-S. Kim, M. Kong, K. Kim, I.-J. Kim, and H.-B. Gu, Journal of Power Sources **171**, 917 (2007).

176 S. Lee, Y. Cho, H.-K. Song, K.T. Lee, and J. Cho, Angewandte Chemie International Edition **51**, 8748 (2012).

177 J.-H. Kim, S.J. Kim, T. Yuk, J. Kim, C.S. Yoon, and Y.-K. Sun, ACS Energy Letters **3**, 3002 (2018).

178 Y. Lee, Energies **12**, 658 (2019).

179 F. Lin, D. Nordlund, I.M. Markus, T.-C. Weng, H.L. Xin, and M.M. Doeff, Energy & Environmental Science **7**, 3077 (2014).

180 M. Kerlau, M. Marcinek, V. Srinivasan, and R.M. Kostecki, Electrochimica Acta **53**, 1385 (2007).

181 G.-L. Xu, Q. Liu, K.K.S. Lau, Y. Liu, X. Liu, H. Gao, X. Zhou, M. Zhuang, Y. Ren, J. Li, M. Shao, M. Ouyang, F. Pan, Z. Chen, K. Amine, and G. Chen, Nature Energy **4**, 484 (2019).

182 W. Liu, Q. Wang, C. Cao, X. Han, J. Zhang, X. Xie, and B. Xia, Journal of Alloys and Compounds **621**, 162 (2015).

183 S. Chae, M. Ko, S. Park, N. Kim, J. Ma, and J. Cho, Energy & Environmental Science **9**, 1251 (2016).

184 J.T. Lee, C. Jo, and M.D. Volder, Proceedings of the National Academy of Sciences **117**, 21155 (2020).

185 J.-H. Kim, N.P.W. Pieczonka, Z. Li, Y. Wu, S. Harris, and B.R. Powell, Electrochimica Acta **90**, 556 (2013).

186 N.J.J. de Klerk and M. Wagemaker, ACS Applied Energy Materials (2018).

187 X. Yu and A. Manthiram, Energy & Environmental Science **11**, 527 (2018).

188 J. Xie, A.D. Sendek, E.D. Cubuk, X. Zhang, Z. Lu, Y. Gong, T. Wu, F. Shi, W. Liu, E.J. Reed, and Y. Cui, ACS Nano **11**, 7019 (2017).

189 G. Chen, B. Peng, R. Han, N. Chen, Z. Wang, and Q. Wang, Ceramics International **46**, 20985 (2020).

190 L. Ma, S. Young, L.D. Ellis, Q. Huang, X. Ma, M. Chatzidakis, H. Li, L. Thompson, A. Eldesoky, C.R.M. McFarlane, G.A. Botton, I.G. Hill, and J.R. Dahn, ACS Applied Energy Materials **1**, 7052 (2018).

191 W. Bao, G. Qian, L. Zhao, Y. Yu, L. Su, X. Cai, H. Zhao, Y. Zuo, Y. Zhang, H. Li, Z. Peng, L. Li, and J. Xie, Nano Letters **20**, 8832 (2020).

192 J.-Z. Kong, C. Ren, G.-A. Tai, X. Zhang, A.-D. Li, D. Wu, H. Li, and F. Zhou, Journal of Power Sources **266**, 433 (2014).

193 W. Liu, M. Wang, X. long Gao, W. Zhang, J. Chen, H. Zhou, and X. Zhang, Journal of Alloys and Compounds **543**, 181 (2012).

194 B. Han, B. Key, S.H. Lapidus, J.C. Garcia, H. Iddir, J.T. Vaughey, and F. Dogan, ACS Applied Materials & Interfaces **9**, 41291 (2017).

195 B. Song, W. Li, S.-M. Oh, and A. Manthiram, ACS Applied Materials & Interfaces **9**, 9718 (2017).

196 W. Cho, S.-M. Kim, J.H. Song, T. Yim, S.-G. Woo, K.-W. Lee, J.-S. Kim, and Y.-J. Kim, Journal of Power Sources **282**, 45 (2015).

197 F. Xin, H. Zhou, X. Chen, M. Zuba, N. Chernova, G. Zhou, and M.S. Whittingham, ACS Applied Materials & Interfaces **11**, 34889 (2019).

198 K. Nie, Y. Hong, J. Qiu, Q. Li, X. Yu, H. Li, and L. Chen, Frontiers in Chemistry **6**, (2018).

199 T. Nakamura, K. Amezawa, J. Kulisch, W.G. Zeier, and J. Janek, ACS Applied Materials & Interfaces **11**, 19968 (2019).

200 T. Famprikis, P. Canepa, J.A. Dawson, M.S. Islam, and C. Masquelier, Nature Materials **18**, 1278 (2019).

201 P.-J. Lian, B.-S. Zhao, L.-Q. Zhang, N. Xu, M.-T. Wu, and X.-P. Gao, Journal of Materials Chemistry A **7**, 20540 (2019).

202 A. Banerjee, X. Wang, C. Fang, E.A. Wu, and Y.S. Meng, Chemical Reviews **120**, 6878 (2020).

203 A.J. Rossini, A. Zagdoun, M. Lelli, A. Lesage, C. Copéret, and L. Emsley, Accounts of Chemical Research **46**, 1942 (2013).

204 A.S.L. Thankamony, J.J. Wittmann, M. Kaushik, and B. Corzilius, Progress in Nuclear Magnetic Resonance Spectroscopy **102-103**, 120 (2017).

205 A.G.M. Rankin, J. Trébosc, F. Pourpoint, J.-P. Amoureux, and O. Lafon, Solid State Nuclear Magnetic Resonance **101**, 116 (2019).

206 C. Song, K.-N. Hu, C.-G. Joo, T.M. Swager, and R.G. Griffin, Journal of the American Chemical Society **128**, 11385 (2006).

207 M.A. Hope, D.M. Halat, P.C.M.M. Magusin, S. Paul, L. Peng, and C.P. Grey, Chemical Communications **53**, 2142 (2017).

208 M. Leskes, G. Kim, T. Liu, A.L. Michan, F. Aussenac, P. Dorffer, S. Paul, and C.P. Grey, The Journal of Physical Chemistry Letters **8**, 1078 (2017).

209 Y. Jin, N.-J.H. Kneusels, L.E. Marbella, E. Castillo-Martínez, P.C.M.M. Magusin, R.S. Weatherup, E. Jónsson, T. Liu, S. Paul, and C.P. Grey, Journal of the American Chemical Society **140**, 9854 (2018).

210 T. Wolf, S. Kumar, H. Singh, T. Chakrabarty, F. Aussenac, A.I. Frenkel, D.T. Major, and M. Leskes, Journal of the American Chemical Society **141**, 451 (2018).

211 D. Jardón-Álvarez, G. Reuveni, A. Harchol, and M. Leskes, The Journal of Physical Chemistry Letters **11**, 5439 (2020).

212 M.A. Hope, B.L.D. Rinkel, A.B. Gunnarsdóttir, K. Märker, S. Menkin, S. Paul, I.V. Sergeyev, and C.P. Grey, Nature Communications **11**, (2020).

213 O.J. Borkiewicz, B. Shyam, K.M. Wiaderek, C. Kurtz, P.J. Chupas, and K.W. Chapman, Journal of Applied Crystallography **45**, 1261 (2012).

214 J.J. Biendicho, M. Roberts, C. Offer, D. Noréus, E. Widenkvist, R.I. Smith, G. Svensson, K. Edström, S.T. Norberg, S.G. Eriksson, and S. Hull, Journal of Power Sources **248**, 900 (2014).

215 W.R. Brant, D. Li, Q. Gu, and S. Schmid, Journal of Power Sources **302**, 126 (2016).

216 O.J. Borkiewicz, K.M. Wiaderek, P.J. Chupas, and K.W. Chapman, The Journal of Physical Chemistry Letters **6**, 2081 (2015).

217 H. Liu, P.K. Allan, O.J. Borkiewicz, C. Kurtz, C.P. Grey, K.W. Chapman, and P.J. Chupas, Journal of Applied Crystallography **49**, 1665 (2016).

218 F. Rosciano, M. Holzapfel, H. Kaiser, W. Scheifele, P. Ruch, M. Hahn, R. Kötz, and P. Novák, Journal of Synchrotron Radiation **14**, 487 (2007).

219 R. Petibon, J. Li, N. Sharma, W.K. Pang, V.K. Peterson, and J.R. Dahn, Electrochimica Acta **174**, 417 (2015).

220 V.A. Godbole, M. Heß, C. Villevieille, H. Kaiser, J.-F. Colin, and P. Novák, RSC Adv. **3**, 757 (2013).

221 H. Liu, F.C. Strobridge, O.J. Borkiewicz, K.M. Wiaderek, K.W. Chapman, P.J. Chupas, and C.P. Grey, Science **344**, 1252817 (2014).

222 Z. Lun, B. Ouyang, Z. Cai, R.J. Clément, D.-H. Kwon, J. Huang, J.K. Papp, M. Balasubramanian, Y. Tian, B.D. McCloskey, H. Ji, H. Kim, D.A. Kitchaev, and G. Ceder, Chem **6**, 153 (2020).

223 K.M. Wiaderek, O.J. Borkiewicz, E. Castillo-Martínez, R. Robert, N. Pereira, G.G. Amatucci, C.P. Grey, P.J. Chupas, and K.W. Chapman, Journal of the American Chemical Society **135**, 4070 (2013).

224 A. Simonov, T. De Baerdemaeker, H.L.B. Boström, M.L.R. Gómez, H.J. Gray, D. Chernyshov, A. Bosak, H.-B. Bürgi, and A.L. Goodwin, Nature **578**, 256 (2020).

225 H. Ji, A. Urban, D.A. Kitchaev, D.-H. Kwon, N. Artrith, C. Ophus, W. Huang, Z. Cai, T. Shi, J.C. Kim, H. Kim, and G. Ceder, Nature Communications **10**, (2019).

226 S. Permien, T. Neumann, S. Indris, G. Neubüser, L. Kienle, A. Fiedler, A.-L. Hansen, D. Gianolio, T. Bredow, and W. Bensch, Physical Chemistry Chemical Physics **20**, 19129 (2018).

227 K.M.Ø. Jensen, X. Yang, J.V. Laveda, W.G. Zeier, K.A. See, M.D. Michiel, B.C. Melot, S.A. Corr, and S.J.L. Billinge, Journal of The Electrochemical Society **162**, 1310 (2015).

228 S.D.M. Jacques, M.D. Michiel, S.A.J. Kimber, X. Yang, R.J. Cernik, A.M. Beale, and S.J.L. Billinge, Nature Communications **4**, (2013).

229 K.W. Chapman, S.H. Lapidus, and P.J. Chupas, Journal of Applied Crystallography **48**, 1619 (2015).

230 H.S. Geddes, H. Blade, J.F. McCabe, L.P. Hughes, and A.L. Goodwin, Chemical Communications **55**, 13346 (2019).

231 V.L. Deringer, C. Merlet, Y. Hu, T.H. Lee, J.A. Kattirtzi, O. Pecher, G. Csányi, S.R. Elliott, and C.P. Grey, Chemical Communications **54**, 5988 (2018).

232 T.Q. Nguyen and C. Breitkopf, Journal of The Electrochemical Society **165**, 826 (2018).

233 S.-M. Park and J.-S. Yoo, Analytical Chemistry **75**, 455 (2003).

234 A. Nickol, T. Schied, C. Heubner, M. Schneider, A. Michaelis, M. Bobeth, and G. Cuniberti, Journal of The Electrochemical Society **167**, 090546 (2020).

235 J.F.B. L. S. Cahill R. P. Chapman and G.R. Goward, J. Phys. Chem. B **110**, (2006).

236 C.V. Chandran and P. Heitjans, in *Annual Reports on NMR Spectroscopy* (Elsevier, 2016), pp. 1–102.

237 I. McClelland, B. Johnston, P.J. Baker, M. Amores, E.J. Cussen, and S.A. Corr, Annual Review of Materials Research **50**, 371 (2020).

238 A.V. der Ven and G. Ceder, Electrochem. Solid-State Lett. **3**, (2000).

239 T.E. Ashton, P.J. Baker, D. Bauer, A.R. Groves, C. Sotelo-Vazquez, T. Kamiyama, T. Matsukawa, K.M. Kojima, and J.A. Darr, Journal of Materials Chemistry A **8**, 11545 (2020).

240 O. Pecher, J. Carretero-González, K.J. Griffith, and C.P. Grey, Chemistry of Materials **29**, 213 (2016).

241 I. McClelland, S.G. Booth, H. El-Shinawi, B.I.J. Johnston, J. Clough, W. Guo, E.J. Cussen, P.J. Baker, and S.A. Corr, ACS Applied Energy Materials **4**, 1527 (2021).

242 Z. Deng, X. Lin, Z. Huang, J. Meng, Y. Zhong, G. Ma, Y. Zhou, Y. Shen, H. Ding, and Y. Huang, Advanced Energy Materials 2000806 (2020).

243 T.L. Burnett and P.J. Withers, Nature Materials **18**, 1041 (2019).

244 D.P. Finegan, M. Scheel, J.B. Robinson, B. Tjaden, I. Hunt, T.J. Mason, J. Millichamp, M.D. Michiel, G.J. Offer, G. Hinds, D.J.L. Brett, and P.R. Shearing, Nature Communications **6**, (2015).

245 L. Wheatcroft, N. Klingner, R. Heller, G. Hlawacek, D. Ozkaya, J. Cookson, and B.J. Inkson, ACS Applied Energy Materials (2020).

246 T.M.M. Heenan, C. Tan, J. Hack, D.J.L. Brett, and P.R. Shearing, Materials Today **31**, 69 (2019).

247 S.R. Daemi, C. Tan, T. Volkenandt, S.J. Cooper, A. Palacios-Padros, J. Cookson, D.J.L. Brett, and P.R. Shearing, ACS Applied Energy Materials **1**, 3702 (2018).

248 X. Lu, A. Bertei, D.P. Finegan, C. Tan, S.R. Daemi, J.S. Weaving, K.B. O'Regan, T.M.M. Heenan, G. Hinds, E. Kendrick, D.J.L. Brett, and P.R. Shearing, Nature Communications **11**, (2020).

249 S.L. Morelly, J. Gelb, F. Iacoviello, P.R. Shearing, S.J. Harris, N.J. Alvarez, and M.H. Tang, ACS Applied Energy Materials **1**, 4479 (2018).

250 A. Quinn, H. Moutinho, F. Usseglio-Viretta, A. Verma, K. Smith, M. Keyser, and D.P. Finegan, Cell Reports Physical Science **1**, 100137 (2020).

251 D. Zeibig, T. Bernthaler, G. Schneider, and S. Freitag, Microscopy and Microanalysis **24**, 1512 (2018).

252 W. Li, A. Dolocan, P. Oh, H. Celio, S. Park, J. Cho, and A. Manthiram, Nature Communications **8**, (2017).

253 E.M. Erickson, W. Li, A. Dolocan, and A. Manthiram, ACS Applied Materials & Interfaces **12**, 16451 (2020).

254 M. Gu, L.R. Parent, B.L. Mehdi, R.R. Unocic, M.T. McDowell, R.L. Sacci, W. Xu, J.G. Connell, P. Xu, P. Abellan, X. Chen, Y. Zhang, D.E. Perea, J.E. Evans, L.J. Lauhon, J.-G. Zhang, J. Liu, N.D. Browning, Y. Cui, I. Arslan, and C.-M. Wang, Nano Letters **13**, 6106 (2013).

255 C.-Y. Chen, T. Sano, T. Tsuda, K. Ui, Y. Oshima, M. Yamagata, M. Ishikawa, M. Haruta, T. Doi, M. Inaba, and S. Kuwabata, Scientific Reports **6**, (2016).

256 E. Fahrenkrug, D.H. Alsem, N. Salmon, and S. Maldonado, Journal of The Electrochemical Society **164**, 358 (2017).

257 J. Hou, R. Girod, N. Nianias, T.-H. Shen, J. Fan, and V. Tileli, Journal of The Electrochemical Society **167**, 110515 (2020).

258 P. Abellan, B.L. Mehdi, L.R. Parent, M. Gu, C. Park, W. Xu, Y. Zhang, I. Arslan, J.-G. Zhang, C.-M. Wang, J.E. Evans, and N.D. Browning, Nano Letters **14**, 1293 (2014).

259 Z. Wang, D. Santhanagopalan, W. Zhang, F. Wang, H.L. Xin, K. He, J. Li, N. Dudney, and Y.S. Meng, Nano Letters **16**, 3760 (2016).

260 D. Chen, S. Indris, M. Schulz, B. Gamer, and R. Mönig, Journal of Power Sources **196**, 6382 (2011).

261 M.I. Nandasiri, L.E. Camacho-Forero, A.M. Schwarz, V. Shutthanandan, S. Thevuthasan, P.B. Balbuena, K.T. Mueller, and V. Murugesan, Chemistry of Materials **29**, 4728 (2017).

262 M.E. Holtz, Y. Yu, D. Gunceler, J. Gao, R. Sundararaman, K.A. Schwarz, T.A. Arias, H.D. Abruña, and D.A. Muller, Nano Letters **14**, 1453 (2014).

263 G. Rong, X. Zhang, W. Zhao, Y. Qiu, M. Liu, F. Ye, Y. Xu, J. Chen, Y. Hou, W. Li, W. Duan, and Y. Zhang, Advanced Materials **29**, 1606187 (2017).

264 R.R. Unocic, R.L. Sacci, G.M. Brown, G.M. Veith, N.J. Dudney, K.L. More, F.S. Walden, D.S. Gardiner, J. Damiano, and D.P. Nackashi, Microscopy and Microanalysis **20**, 452 (2014).

265 G. Xu, X. Zhang, M. Liu, H. Li, M. Zhao, Q. Li, J. Zhang, and Y. Zhang, Small **16**, 1906499 (2020).

266 Y. Xie, H. Wang, G. Xu, J. Wang, H. Sheng, Z. Chen, Y. Ren, C.-J. Sun, J. Wen, J. Wang, D.J. Miller, J. Lu, K. Amine, and Z.-F. Ma, Advanced Energy Materials **6**, 1601306 (2016).

267 J. Wang, Y.-chen K. Chen-Wiegart, and J. Wang, Nature Communications **5**, (2014).

268 D.J. Miller, C. Proff, J.G. Wen, D.P. Abraham, and J. Bareño, Advanced Energy Materials **3**, 1098 (2013).

269 Y. Zhao, P. Stein, Y. Bai, M. Al-Siraj, Y. Yang, and B.-X. Xu, Journal of Power Sources **413**, 259 (2019).

270 A. Singer, M. Zhang, S. Hy, D. Cela, C. Fang, T.A. Wynn, B. Qiu, Y. Xia, Z. Liu, A. Ulvestad, N. Hua, J. Wingert, H. Liu, M. Sprung, A.V. Zozulya, E. Maxey, R. Harder, Y.S. Meng, and O.G. Shpyrko, Nature Energy **3**, 641 (2018).

271 W. Huddleston, F. Dynys, and A. Sehirlioglu, Journal of the American Ceramic Society **103**, 1527 (2019).

272 L.S. de Vasconcelos, N. Sharma, R. Xu, and K. Zhao, Experimental Mechanics **59**, 337 (2018).

273 R. Xu, H. Sun, L.S. de Vasconcelos, and K. Zhao, Journal of The Electrochemical Society **164**, 3333 (2017).

274 D. Dang, Y. Wang, and Y.-T. Cheng, Journal of The Electrochemical Society **166**, 2749 (2019).

275 W.C. Oliver and G.M. Pharr, Journal of Materials Research **7**, 1564 (1992).

276 G.R. Anstis, P. Chantikul, B.R. Lawn, and D.B. Marshall, Journal of the American Ceramic Society **64**, 533 (1981).

277 J. Wolfenstine, J.L. Allen, T.R. Jow, T. Thompson, J. Sakamoto, H. Jo, and H. Choe, Ceramics International **40**, 13673 (2014).

278 M. Qu, W.H. Woodford, J.M. Maloney, W.C. Carter, Y.-M. Chiang, and K.J.V. Vliet, Advanced Energy Materials **2**, 940 (2012).

279 P. Yan, J. Zheng, M. Gu, J. Xiao, J.-G. Zhang, and C.-M. Wang, Nature Communications **8**, (2017).

280 J.J. Vlassak and W.D. Nix, Journal of the Mechanics and Physics of Solids **42**, 1223 (1994).

281 H. Tavassol, E.M.C. Jones, N.R. Sottos, and A.A. Gewirth, Nature Materials **15**, 1182 (2016).